Journal of Structural Geology 37 (2012) 36–52

Contents lists available at SciVerse ScienceDirect

Journal of Structural Geology

journal homepage: www.elsevier.com/locate/jsg

Hot fluid pumping along shallow-level collisional thrusts: The Monte Rentella Shear Zone, Umbria Apennine, Italy

F. Meneghini [a,*], F. Botti [a], L. Aldega [b], C. Boschi [c], S. Corrado [d], M. Marroni [a,c], L. Pandolfi [a,c]

[a] Dipartimento di Scienze della Terra, Università di Pisa, Via S. Maria 53, 56126 Pisa, Italy
[b] Dipartimento di Scienze della Terra, Sapienza Università di Roma, P.le Aldo Moro 5, 00185 Roma, Italy
[c] Istituto di Geoscienze e Georisorse, Centro Nazionale delle Ricerche, Via Moruzzi 1, 56124 Pisa, Italy
[d] Dipartimento di Scienze Geologiche, Università Roma TRE, Largo San L. Murialdo 1, 00146 Roma, Italy

ARTICLE INFO

Article history:
Received 19 April 2011
Received in revised form
31 January 2012
Accepted 2 February 2012
Available online 19 February 2012

Keywords:
Shallow level collisional thrusts
Fluid-driven fault-fracture mesh
Vitrinite reflectance
C and O stable isotopes
Northern Apennines

ABSTRACT

The characteristics of a shallow-level shear zone that is representative of the deformation in the external sectors of the Northern Apennine fold-and-thrust belt are described. The characterization involved an integrated approach using microstructural analysis of deformation fabrics, vitrinite reflectance measurements, XRD analysis on clay minerals and carbon and oxygen stable isotopes analyses. This data set provides the evidence that the thrust was active at very shallow depths (ca. less than 3 km), with maximum paleotemperatures ranging from 60° to 100–110 °C. The regime during fault activity evolved through cycles of compaction and dilation linked to transient build up of fluid overpressure and injection. The alternating cycles of fluids supply generated a fault-fracture mesh with a complex network of blocky and striped veins that formed at temperatures ranging from 150° to 200 °C, not compatible with the conditions in the host rocks. This evidence implies that the shear zone was flooded by hot fluids coming upward from diagenetic and low-grade metamorphic dehydration of clay minerals active at deeper structural levels. The fluids were thus highly channelled and focused where deformation also focused, producing a local pronounced isotopic difference between fluids and host rock.

1. Introduction

The hydrogeologic characteristics of fault zones are matter of deep structural and economic geologic interest, particularly during the last half of the century, because of their crucial role in influencing heat and mass transport, healing processes, overall fault strength, fault mechanical evolution and economic importance. After all, hydrothermal mineral deposits, as well as the production of hydrocarbons and gas, rely on the availability of large volumes of fluids that in many cases flowed along faults (e.g. Newhouse, 1942; Hubbert and Rubey, 1959; Fyfe et al., 1978; Hunt, 1990; Cox et al., 1991, 2001; Fournier, 1991; Sibson, 1990, 1994; 1996, 2001; Law et al., 1998; Hillis, 2001; Leader et al., 2010 and references therein). In particular, starting from the work by Hubbert and Rubey (1959), the feedbacks between cycling of stress and fluid pressure have interested many scientists, and the fluid migrations with pressures well in excess of hydrostatic, are considered to play a fundamental role in weakening low and high displacement fault zones, because of the efficiency of high pressure fluids for reducing the effective normal stress prior to slip. The effects of fluid-rock interaction along faults are also crucial at the tectonic scale, as first suggested by Davis et al. (1983), in the context of the dynamics of accretionary prisms (e.g. Saffer and Bekins, 2002 and references therein).

Since Hubbert and Rubey's contribution, many field, laboratory, and geophysical studies have worked to unravel the mechanical involvement of fluids in the faulting process. Evidence of fluid circulation along fault-related fracture systems have come from *in situ* measurements in active tectonic regions (thermal, chemical and porosity anomalies, negative seismic reflectors: Shipley et al., 1995; Bangs et al., 1999, 2004; Brown et al., 2001), and from the occurrence of mineral-infused vein systems in the faults of ancient orogenic belts (e.g. Labaume et al., 1991; Fisher and Brantley, 1992; Moore and Vrolijk, 1992; Chester et al., 1993; Fisher, 1996; Lewis et al., 2000; Collettini at al., 2006; Meneghini et al., 2007). Special attention has been devoted to the relationships between fluids flow and pore fluid pressure with the seismic cycle (e.g. Hill, 1977; Ramsay, 1980; Sibson, 1987, 1996, 1990; Cox et al., 1991; Chester

* Corresponding author.
E-mail addresses: meneghini@dst.unipi.it (F. Meneghini), fbotti@dst.unipi.it (F. Botti), luca.aldega@uniroma1.it (L. Aldega), c.boschi@igg.cnr.it (C. Boschi), corrado@uniroma3.it (S. Corrado), marroni@dst.unipi.it (M. Marroni), pandolfi@dst.unipi.it (L. Pandolfi).

0191-8141/$ – see front matter © 2012 Elsevier Ltd. All rights reserved.
doi:10.1016/j.jsg.2012.02.004

et al., 1993; Evans and Chester, 1995; Hickman et al., 1995; Faulkner and Rutter, 2001; Meneghini and Moore, 2007; Rowe et al., 2009).

The coupling of structural and geophysical analyses of fluid-infused faults with other laboratory-based techniques such as fluid inclusion studies, isotopic and geochemical characterization of veins infillings, cathodoluminescence analyses, have confirmed that fluids can circulate via intergranular flow or be highly channelled; they can either have a local origin, or they can move over distances of hundreds of kilometres along faults of regional extent (e.g. fluids released at depth by low-grade metamorphic reactions in sedimentary rocks, see Moore and Saffer, 2001); and they can interact differently with the surrounding rocks depending on the water/rock volume ratio (Fyfe and Kerrich, 1985; Moore et al., 1990; Kastner et al., 1991; Kirschner et al., 1995; Conti et al., 2001; Brown et al., 2001; Goldstein et al., 2005; Hilgers et al., 2006; Vannucchi et al., 2010 and references therein). In line with these contributions, we have conducted a multidisciplinary study on a well-exposed shallow shear zone that is responsible for thrust sheet development during the building of the Apennine collisional prism, and host to a complex system of calcite veins. To reconstruct the structural and temperature fluid rock-interaction during shear zone development, we performed a detailed field and microstructural analysis of the Monte Rentella shear zone structure and deformation fabrics, including vitrinite reflectance measurements, XRD analysis on clay minerals (composition of mixed-layer illite-smectite) and carbon and oxygen stable isotopes analyses. The combined use of vitrinite reflectance and mixed-layer illite-smectite, which is one of the best approaches for unravelling the maximum burial of sedimentary basins in fold-and-thrust belt (Corrado et al., 2005; Aldega et al., 2007, 2011), was applied to regionally contextualize this zone in the framework of the Apennine collisional belt, and to constrain the depth and temperature conditions during fault activity. Stable isotopes were used to identify fluid sources, estimate the temperatures of vein formation and unravel any fluid-rock interaction. The comparison of $\delta^{18}O$ and $\delta^{13}C$ between vein fillings and host rock, and its use with petrological, geological and structural analyses, allowed us to speculate on the origin of the fluids and their interaction with deformation.

2. Geologic setting

The eastern side of the Northern Apennines, corresponding to the Umbria-Marche areas (Fig. 1), is characterized by a fold-and-thrust belt built since Oligocene time, after the closure of the oceanic basin and the collision between the continental margins of the Adria and Europe plates (Marroni et al., 2010 and references therein). The fold-and-thrust belt originated during the progressive migration of the deformation front towards the eastern domains of the Adria plate (e.g., Costa et al., 1998; Barchi et al., 2001). This evolution was associated with the development of foredeep and piggy-back basins of different ages that were progressively incorporated into the belt. As a result, a pile of Adria-derived tectonic units was detached at different structural levels and subsequently deformed by E- to NE-verging thrusts and associated folds (e.g., Barchi et al., 1998). Contractional tectonics was followed by an extension, that caused the development of marine to continental basins bordered by high angle normal faults, segmenting the pre-existing structural stack of tectonic units (e.g. Lavecchia et al., 1987 and Pauselli et al., 2006).

The Lago Trasimeno area (Umbria, Central Italy) is a good study site for structures formed prior to the extensional phase (Fig. 2). Here, the Tuscan Nappe thrusts onto the Umbria-Romagna Unit, which are both derived from different sectors of the Adria plate (Fig. 3). Whereas the Tuscan Nappe originated from the western-most area of the Adria continental margin, the Umbria-Romagna Unit is interpreted as paleogeographically derived from the inner-most zones. Recent field mapping and data collection in the Lago Trasimeno area by Barsella et al. (2009) revealed the occurrence of additional thrust sheets (Sansepolcro-Monte Filoncio and Rentella Unis) between the Tuscan Nappe and Umbria-Romagna Unit (Figs. 2 and 3). Among them, the Rentella Unit is derived from an area originally interposed between the Tuscan and Umbria-Marche units (Barsella et al., 2009). Accordingly, the data collected in the Lago Trasimeno area by Barsella et al. (2009) indicate that the deformation of the Tuscan, Tuscan-Umbria and Umbria-Marche sectors occurred during Aquitanian, Burdigalian and Langhian times, respectively. In addition, scattered "klippen" of the Ligurian units, i.e. the remnants of the oceanic and transitional units belonging to the Late Cretaceous-Middle Eocene accretionary wedge, are identified at the top of the Tuscan Nappe.

The succession of the Rentella Unit includes Rupelian-Aquitanian varicoloured pelagic and hemipelagic marls (Monte Rentella Formation) conformably topped by Aquitanian-Burdigalian siliciclastic turbidites (Montagnaccia Formation), representing the foredeep deposits. This succession is arranged in a stack of imbricate slices bounded by N-S striking thrusts that show ramp-and-flat geometry (Fig. 2). Both boundaries and internal thrusts in the imbricate system are marked by cataclastic shear zones that are metres thick. The studied Monte Rentella Shear Zone (hereafter reported as MRSZ) occurs at the edge of one of the slices. Thrusts can include meso- to mega-scale fault-propagation folds, with sub-horizontal axis striking NW-SE to N-S. These folds, showing concentric geometry, are frequently asymmetric with a well-developed SW-dipping back-limb, whereas the forelimb dips vertically or is overturned. Their axial-plane foliation can be described as a disjunctive cleavage in the pelitic and marly fine-grained lithotypes that is variably spaced in the coarse-grained lithotypes, such as the sandstones.

3. The Monte Rentella collisional thrust in the regional context

Vitrinite reflectance and XRD clay minerals analyses were performed across the studied thrust as part of a regional-scale sampling process, to estimate maximum paleotemperatures and the sedimentary/tectonic burials experienced by the rocks, and to reconstruct the geometry and structure of the units composing the eastern side of the Lago Trasimento area before the extensional development of the Trasimeno basin (Fig. 2). A brief description of these data and related interpretation is helpful to better place the Rentella Unit and the MRSZ in this sector of the Apenninic collisional prism.

For vitrinite reflectance analysis, whole-rock samples and picked coaly particles were collected from sandstone and siltstone lithologies across the section AB of Fig. 2, and in the Montagnaccia Formation of the Rentella Unit. For each sample, we selected only slightly fractured and/or altered vitrinite fragments with grain-size of at least 5 μm, on which at least 20 measurements were performed (Borrego et al., 2006). Mean reflectance (R_o%) and standard deviation values were calculated from measurements. For XRD analysis of pelitic fraction of sediments, randomly-oriented whole-rock powders and oriented <2 μm grain-size fractions were run by a Scintag X1 XRD system (CuKα radiation) at 40 kV and 45 mA. Expandability measurements for both illite-smectite (I-S) and chlorite-smectite (C-S) mixed layer minerals were determined according to Moore and Reynolds (1997), using the delta two-theta method after decomposing the composite peaks between 9 and 10°2θ and 16–17°2θ for I-S and between 10 and 12.3°2θ and 25–26°2θ for C-S using Pearson VII functions.

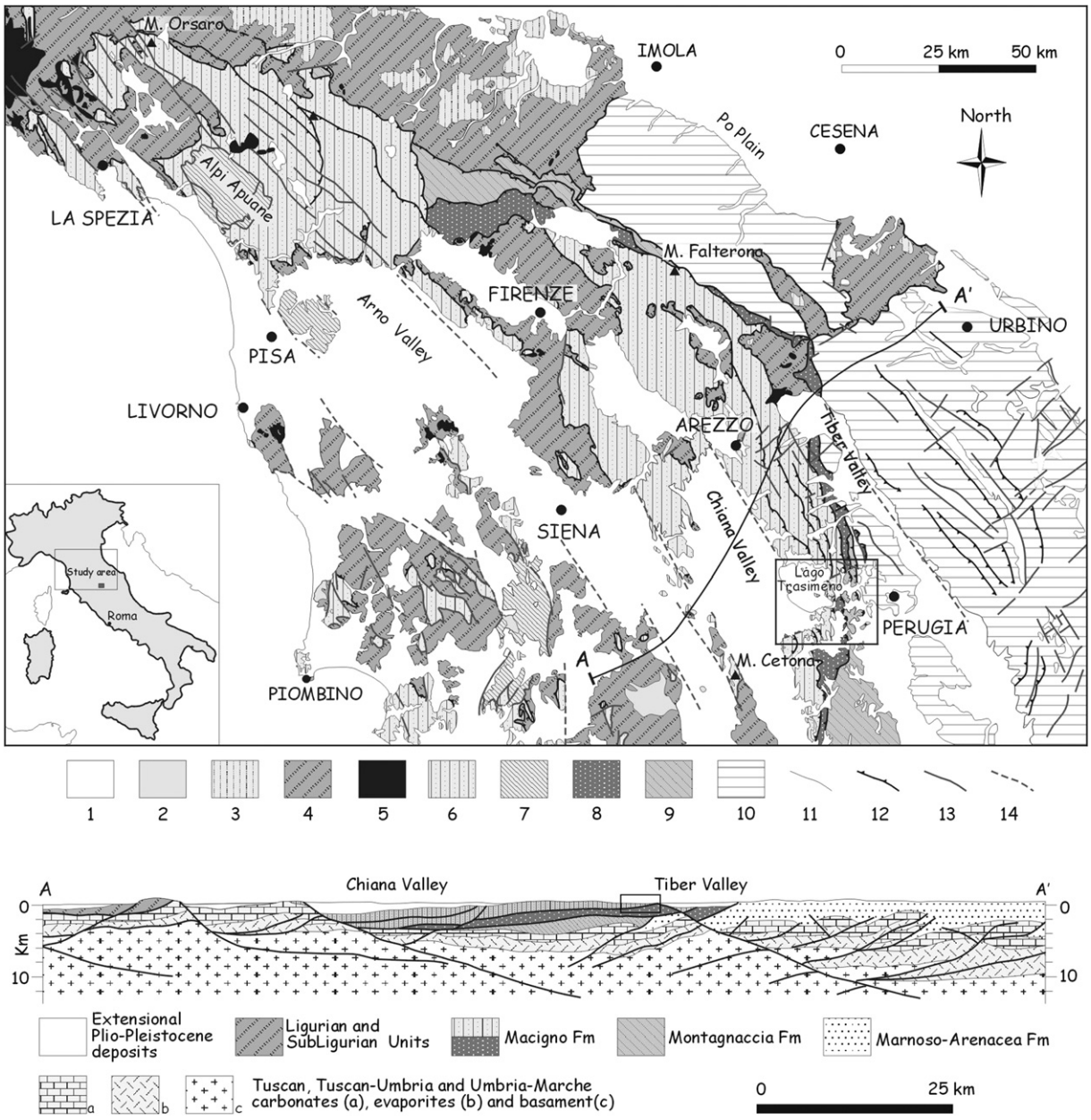

Fig. 1. Simplified structural sketch map of the Northern Apennines from Tuscan-Emilian Apennine to the Trasimeno Lake area and regional cross-section, showing the relationships between main tectonic units: (1) Neogene-Quaternary deposits of the Po Plain and Inner Tuscany; (2) volcanic rocks of the southern Tuscany; (3) Epiligurian Succession; (4) Ligurian Units; (5) Ophiolites of the Ligurian Units. (6) Tuscan Nappe; (7) Tuscan metamorphic units; (8) Acquerino and Sansepolcro-Monte Acuto Units; (9) Carigiola and Rentella Units; (10) Umbria-Romagna Unit; (11) stratigraphic boundary, (12) major thrusts; (13) faults; (14) buried fault. Boxes in map and section show location of map and cross section of Fig. 2, respectively.

The paleotemperatures conversion for vitrinite reflectance data was obtained using the equation proposed by Barker and Pawlewicz (1994). Concerning clay mineralogy, I-S data were converted into paleotemperatures adopting the Basin Maturity Chart of Merriman and Frey (1999).

Analysed kerogen in the turbiditic units of the entire area is generally abundant, homogenous and mainly composed of well-preserved macerals that are for the most part derived from wooden fragments of continental origin, belonging to the humite-vitrinite group and in particular collotelinite and telinite fragments (Stach et al., 1982). Generally, one cluster of Ro values was recognised on each sample, suggesting only one population of indigenous fragments. Samples from the entire area are characterized by a Gaussian distribution of Ro measurements (Fig. 4) with mean values between 0.30 and 0.70%, corresponding to the immature to mid-mature stages of hydrocarbon generation (Fig. 5).

Fig. 6 summarizes the overburden reconstructed, from the paleotemperature data, for the analysed sector of the Lago Trasimeno and for the MRSZ, moving from the SW to the NE along the cross sections of Fig. 2. Using a geothermal gradient of 30 °C/km and a surface temperature of 10 °C, tectonic burial depths ranging from 2 km to 3 km are estimated along the cross section. The paleotemperature recorded in the Rentella Unit and, particularly, across the MRSZ section, can be placed in a regional scenario of deformation and thrust sheets migration across the Apenninic belt. According to their structural position (Figs. 2–5), in fact, the samples from the Rentella units lies between the highest measured values of the Macigno Formation (R_o% ca. 0.70%), belonging to the

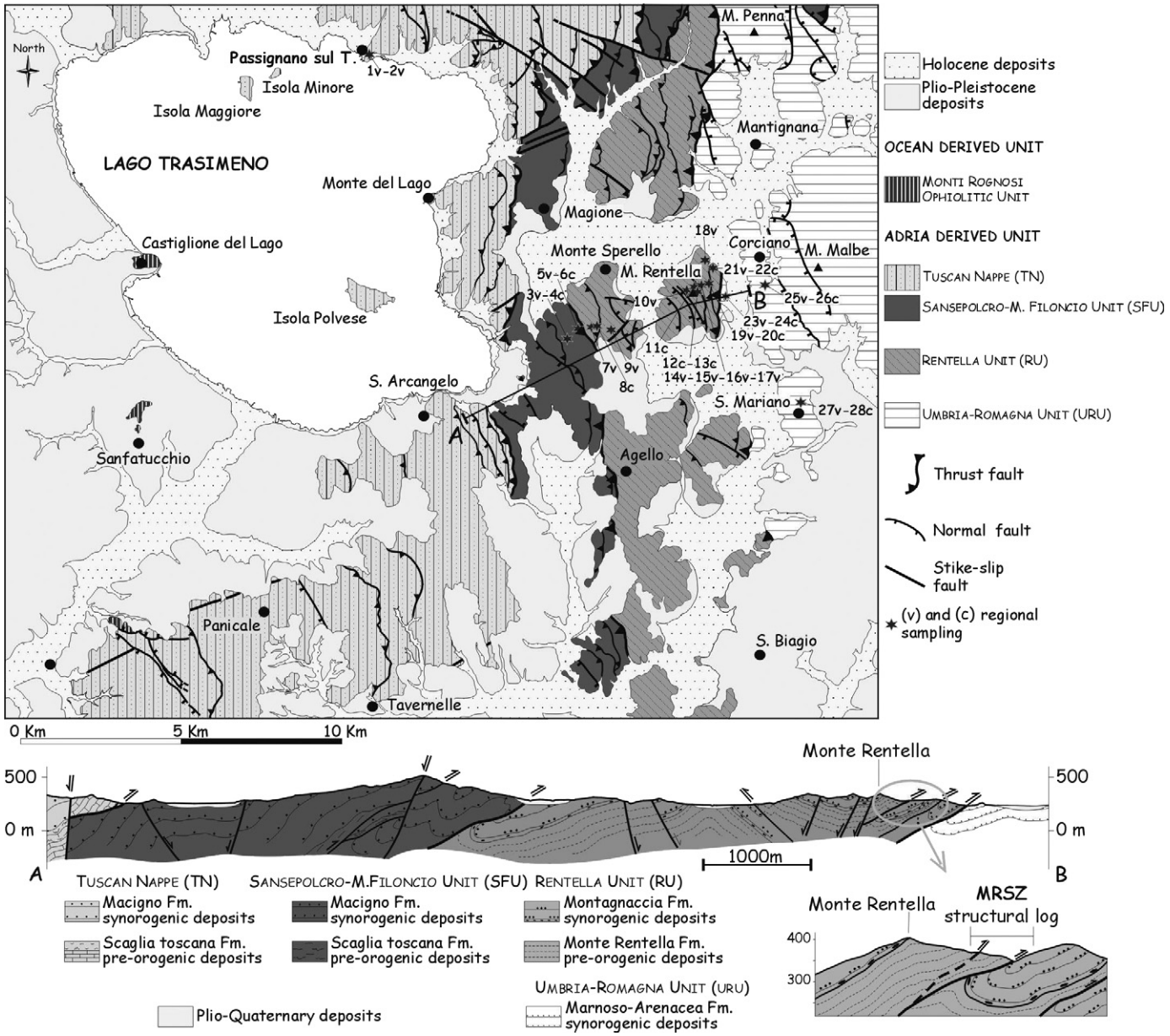

Fig. 2. Structural sketch-map of the Lago Trasimeno area, related geological cross section (A-B traces of cross section), and close-up view of MRSZ outcrop area, with the location of the structural log of Fig. 6 indicated. Samples location in the map: (v) stands for vitrinite reflectance and (c) for clay mineralogy sampling.

innermost and structurally uppermost unit of the thrust sheet system (Tuscan Unit), and the lowest values, recorded in the siliciclastic foredeep deposits of the Umbria-Romagna Unit (R_o% ranging from 0.517%, right below the Rentella Unit basal thrust, to 0.392% in a eastward direction), representing the external and lowermost units of the Lago Trasimeno section. These data suggest for this transect of the collisional belt, a sequence of thrusting and thrust-sheet development of piggy-back type, with deformation moving from the internal to the external portion of the belt. In this scenario, the Rentella Unit overburden ranges from 2.5 km, at the footwall of the Sansepolcro-Monte Filoncio Unit, to around 2 km in the frontal part of the unit (Fig. 6).

The base of the MRSZ, which is sampled in seven localities from the footwall damage zone to the undeformed (14v–20v in Fig. 5), shows R_o% data of indigenous fragments gradually increasing structurally downward from the thrust, with mean values between 0.318 and 0.517%. We consider the values around 0.3% as underestimating maximum paleotemperatures, given that they are around the limit of reliability of the method of vitrinite reflectance (Dow, 1977), and of the application of published equations in paleotemperatures conversion (Dalla Torre et al., 1997). Therefore, we consider the values between 0.4 and 0.5% to be indicative of the thermal maturity experienced by the Montagnaccia Formation below the MRSZ. Calculated paleotemperatures are therefore between 60 and 80 °C (Barker and Pawlewicz, 1994).

XRD data show that whole-rock samples from different structural and stratigraphic positions display similar mineral assemblages. Calcite, quartz, Na-plagioclase and phyllosilicates represent the main constituents of both marls of the Rentella Unit and shales from the Macigno Formation. Observed differences in mineral abundance are mainly lithology-related (Table 1).

In the <2 μm grain-size fraction of the Rentella Unit's samples, the Miocene siliciclastic deposits of the Montagnaccia Formation are characterized by illite, mixed layers I-S and C-S and small

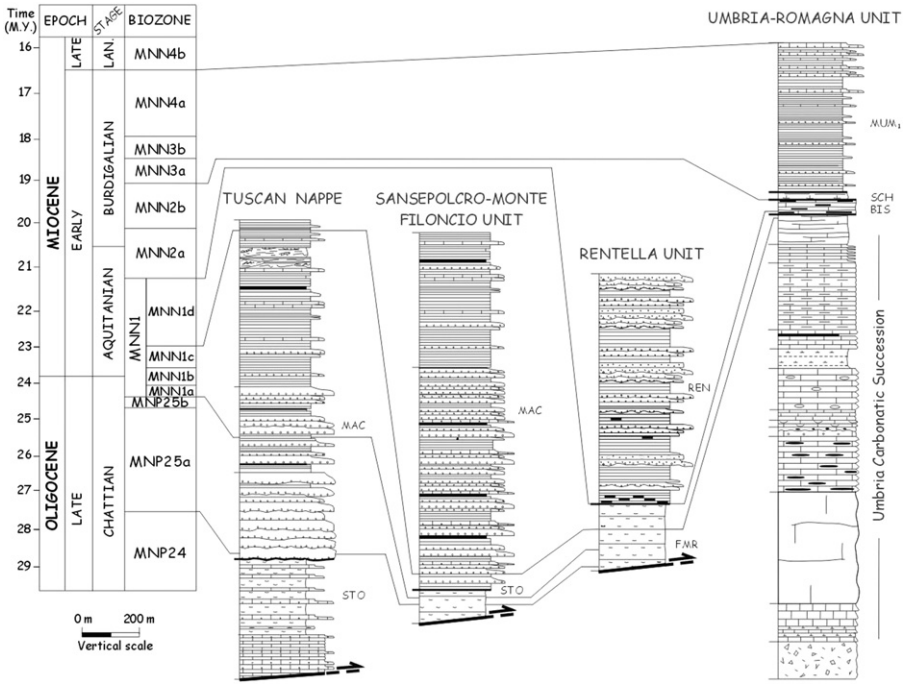

Fig. 3. Lithostratigraphic sections of main units cropping out in the Umbrian sector of the Apennines, and their geometrical relationships. A stratigraphic scheme is also presented.

amount of chlorite. A similar illite and I-S-rich composition occurs in the hemipelagic deposits of the Rentella Formation. Their <2 μm grain-size fraction is also composed of mixed layers C-S with a chlorite content between 52 and 60%. No positive correlation was found between deformation and illite content in mixed layer I-S: the strongly deformed samples with penetrative foliation from the shear zone, as well as those slightly deformed collected farther away from the MRSZ, display short-range ordered I-S with an illite content between 63 and 76%. Both deformed and slightly deformed samples show an I-S composition that suggests maximum paleotemperatures not higher than 100–110 °C at the boundary between early and late diagenesis (Merriman and Frey, 1999).

By combining the two geothermometers, the maximum temperature range estimated for the Rentella Unit (and the MRSZ), is between 60 °C and 100–110 °C.

4. MRSZ structure and mineralization

To document the detailed evolution of the fault and its interaction with fluid migration along the slipping surfaces, a structural log (Fig. 7) across the MRSZ structure was constructed based on a field description of the MRSZ at the cm to mm scale, including description and distribution of deformation fabrics, measurements of foliation, shear and fracture planes, measurements of vein attitudes, and a quantitative definition of vein distribution throughout the outcrop. Across the MRSZ, samples of wall rock were collected for microstructural analyses, together with veins samples used to characterize vein composition, texture infilling and relationships with deformation. Rock samples and associated veins from the core zone and the hangingwall damage zones of the MRSZ structure were also collected to perform stable isotope analyses (O, C).

4.1. MRSZ architecture

The exposed MRSZ is a ramp of the thrust system deforming the Rentella Unit. It crops out with continuous exposures along the eastern side of the Monte Rentella (Umbria Region) and juxtaposes the Rupelian Monte Rentella Formation over the Aquitanian-Burdigalian Montagnaccia Formation (Fig. 2). This shear zone evolved during the thrusting of the Rentella Unit onto the Umbria-Marche Domain and is Burdigalian-Langhian in age.

Thrust strikes approximately N 160°–N 170°, dipping 60°–70° towards SW, and it shows an NE sense of tectonic transport in agreement with the Apennine collisional structure. The mountain flank trends almost normally to fault strike, providing outcrop suitable for a detailed analysis of structures and active deformation mechanisms across the shear zone (Fig. 2).

Both hangingwall and footwall transitions to the undeformed rocks are well exposed, and the thrust is marked by a ca. 50 m thick disrupted zone (Fig. 7). Disruption concentrates in the marls of the

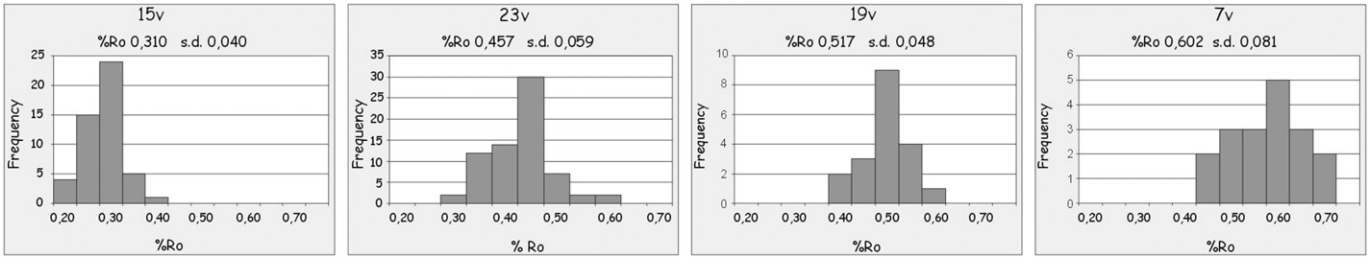

Fig. 4. Examples of Gaussian distribution of Ro measurements on samples collected in Rentella Unit (15v, 23v, 19v) and Umbria-Romagna Unit (7v).

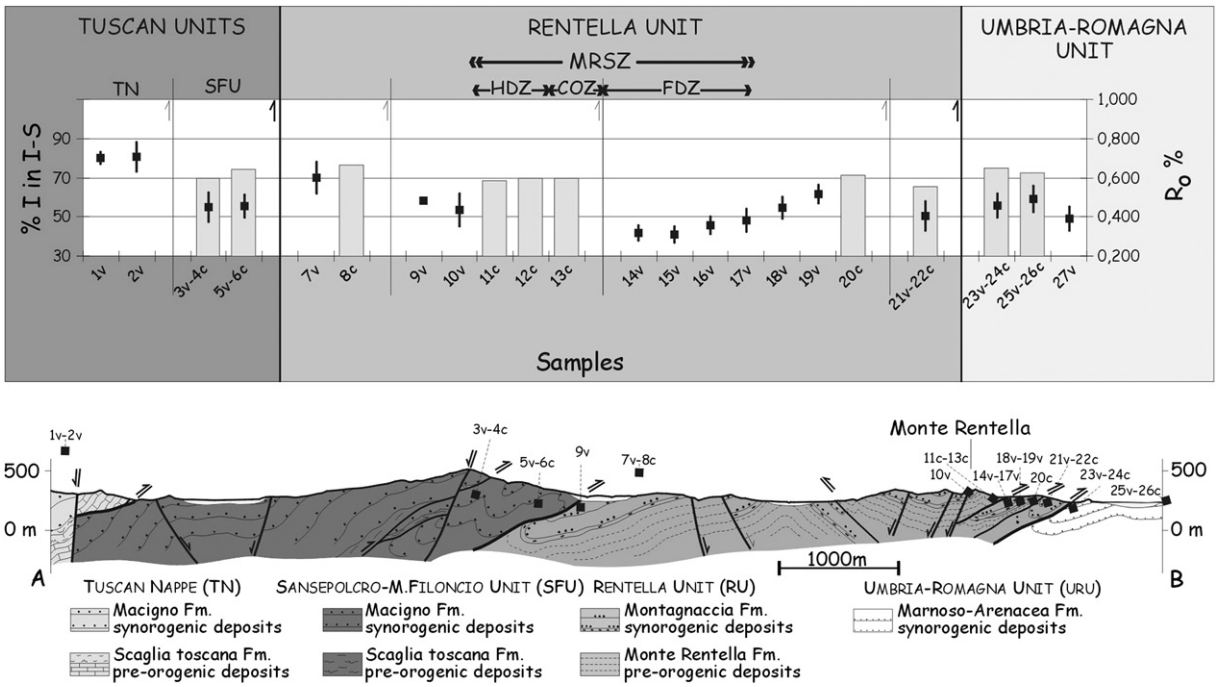

Fig. 5. Illite content in mixed layer illite-smectite (black squares with error bars) and %Ro (grey blocks) values in analysed units (TN: Tuscan Nappe, SFU: San Sepolcro-M. Filoncio) and across the MRSZ (hangingwall (HDZ) and footwall (FDZ) damage zones and core zone (CO). Location of samples for vitrinite measurements (v) and X-ray diffraction of clay minerals (c) shown in Fig. 2.

Monte Rentella Formation. Therefore, the intensity of deformation and meso-scale fabric development, as measured across the constructed structural log (Fig. 7), are distributed asymmetrically for the MRSZ, with an about 3.5 m thick core zone (COZ) bounded by strikingly different footwall and hangingwall damage zones. The core is where most deformation is accommodated, featuring the greatest density of deformation-related structures (Caine and Forster, 1999).

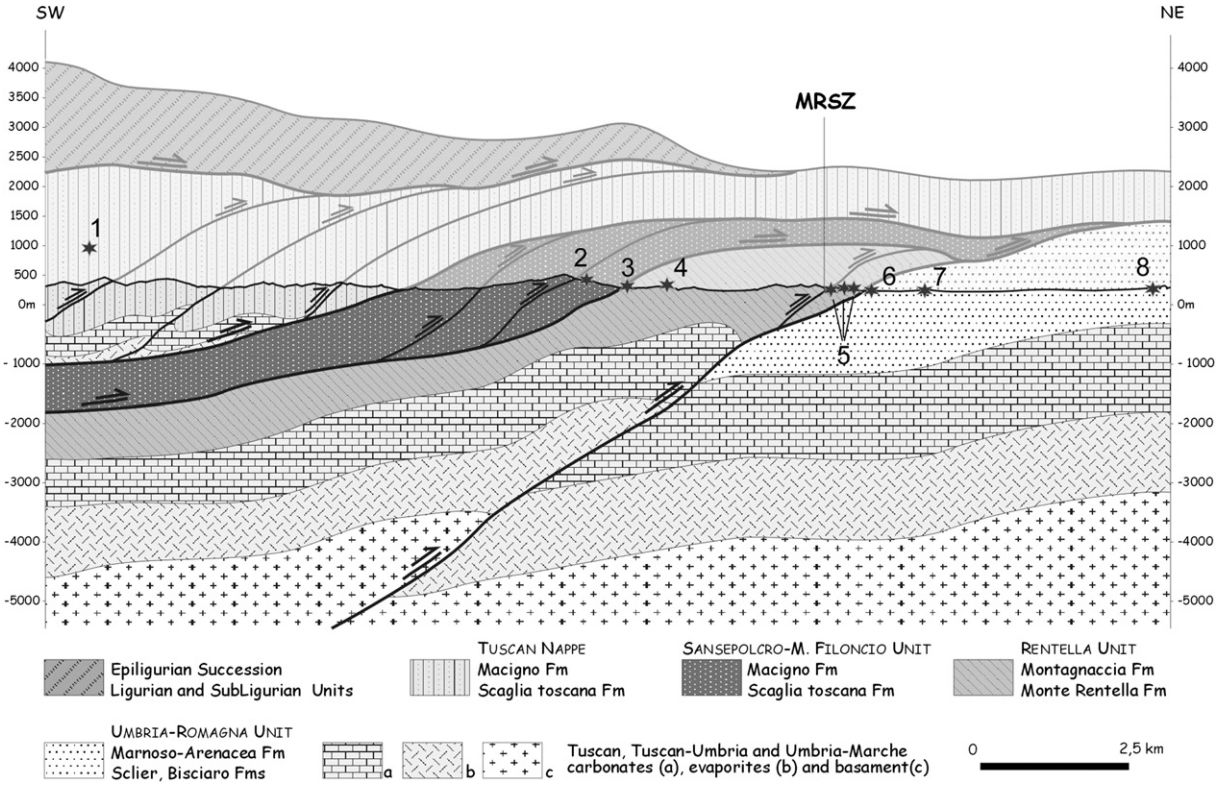

Fig. 6. –Estimated tectonic burial prior to the extension of the Rentella Unit using vitrinite reflectance and mixed layer I-S data. Stars are vitrinite samples locations (see also map in Fig. 2, and scheme of Fig. 5): (1) Tuscan Units (1v, 2v); (2) San Sansepolcro-Monte Filoncio Unit (3v, 5v); (3) Rentella Unit at the footwall of the Sansepolcro-Monte Filoncio Unit (7v); (4) Rentella Unit (10v); (5) base of MRSZ (14v–17v); (6), (7), (8) Umbria-Romagna Unit, from the internal to the external sectors (23v, 25v, 27v).

Table 1
XRD quantitative analyses of the whole-rock composition and the <2 μm grain-size fraction. Note that non-clay minerals which have been identified in the <2 μm grain-size fraction were not included in the quantitative analysis of the oriented aggregates and data refer to the phyllosilicates group only. The amounts of clay minerals were not recalculated into percentages of bulk rocks, but represent the content of the separated phyllosilicates-size fraction.

Sample	Formation	Rock type	Mineralogy of the whole-rock (%wt.)						X-ray quantitative analysis of the <2 μm grain-size fraction (%wt.)					%I in I-S	%C in C-S
			Qtz	Cal	Dol	Ab	Phy	Py	I	I/S	C/S	K	Chl		
24	Marnoso	Marl	13	11	2	21	52	1	41	14		10	35	75	
26	Arenacea Fm	Siltstone	12	23	4	15	46		65	18	14		3	73	60
8	Montagnaccia	Marl	7	64		3	26		58	22	19		1	76	55
22	Fm	Marl	4	57		2	37		57	29	12		1	76	55
22(1)		Marl	10	25		7	58		65	25	10			65	55
11	Monte	Marl	4	55		1	40		62	29	6		3	68	55
11(1)	Rentella Fm	Marl	4	69		1	26		69	18	10	1	2	68	60
12		Marl	5	55		3	37		60	33	2	3	2	70	52
12(1)		Marl	5	57		4	34		58	22	14	2	4	70	60
13		Marl	5	59		2	34		60	26	12	1	1	63	55
13(1)		Marl	5	59		2	34		60	21	6	6	7	70	50
20		Marl	6	60		4	30		61	30	2		7	72	60
6	Macigno Fm	Shale	3	1		1	95		41	59				74	
4		Marl	9	22		12	57		65	27	7		1	70	60

The footwall damage zone (FDZ) developed in amalgamated beds of massive sandstones from the Montagnaccia Formation, for a thickness of about 28.5 m. Deformation is accommodated by a well-developed spaced dissolution foliation with a spacing from 2 to 5 cm. Fractures are arranged in 3 main sets of planes (Fig. 8): two NE-dipping sets both striking N 150°–N 180°, with different inclination (30° and 75°) and a third set striking N 130°–160°, dipping 20°–40° towards the SW. This last set is generally ornamented by a strong striation lineation striking N 40°–60° and showing a top-to-NE sense of shear, coherent with that inferred at map-scale for the thrust (Fig. 8c). These sets are interpreted in terms of synthetic and antithetic Riedel shear planes, developed to accommodate strain at the footwall, where the NE-dipping planes are R- and R′-Riedel planes associated with a main shear surface oriented as the cluster dipping towards the SW, and indicating a top-to-the-NE sense of shear. Deformation in the sandstones also features development of cataclastic shear zones (Fig. 9a), visible at all scales, and characterized by grain-size reduction at micro-scale (Fig. 9b). Scattered pressure solution seams are also associated with the shear zones.

The core zone in the Monte Rentella Formation marls shows extensive deformation with fabrics including many typical features of brittle shear zones in pelitic to marly lithotypes (Figs. 9–11), such as a strongly penetrative scaly foliation, Riedel-type sets of structures, shear-related asymmetric folds and extensive veining. Core zone boundaries are sharp, represented by tectonic surfaces.

Similar to S-C structures in the ductile regime, a P-type foliation is associated with *Y*-shear surfaces, visible at the meso- to the micro-scale, with Y-shear planes deforming and cutting the P-foliation surfaces (Fig. 11a). Y-shear surfaces are generally arranged parallel to the mean shear zone boundaries, striking N 160°–170° with a dipping of 40–50° towards SW (compare with geologic section), and therefore fitting also with the SW-dipping surfaces detected in the sandstones (Fig. 8). Average strike of the foliation ranges N 110°–N 160° and foliation planes locally show polished and striated surfaces. P-Y structures arrangement indicates a top-to-E-NE sense of shear, according with the main thrust vergence. Both P and Y surfaces are infused with calcite veins.

The scaly nature of the foliation in marls is defined by an anastomosing set of fracture planes, with spacing smaller than 1 mm (Fig. 9c and Fig. 11a), marked by variably continuous microscopic pressure solution seams, also evidenced by partial dissolution of foraminifera along the seams. Also, foraminifera are generally elongated along foliation or deform as delta-type objects typical of ductile shear zones (Fig. 9d).

Foliation planes as well as veins are markedly folded in all exposures. The folds are strongly asymmetric and show variable geometry, from open to tight to isoclinal, without any visible axial-plane foliation (Fig. 9c). Limbs are frequently necked and boudinaged. Fold axes trend N 140°–N 170° with plunges clustered towards the NW and SE (Fig. 10a). Fold asymmetry is clearly related to the axes plunge: NW-plunging fold axes characterize NE-facing folds, whereas SE-plunging axes are connected with SW-facing folds. This fold arrangement is typical of shear zones with a large component of simple shear. Given this interpretation, the cylindrical best fit of the fold axes represents the plane of main shear to which the folds are related (Fig. 10b), and correspond approximately to both the average attitude of the main fault and to the Y-planes (N 162° 45 NNE – Fig. 10b).

The HDZ developed in the central-upper portion of the Monte Rentella Formation, also deforming marly lithologies. The transition from HDZ to both COZ and undeformed Monte Rentella Formation is sharp, marked by thin (on the order of millimetres) gouges layers arranged along Y-shear surfaces, and confirmed also by biostratigraphic data of calcareous nannofossil content. Sampling across this zone indicates boundaries defined by low-angle reverse faults that each juxtapose rock of different age: 1) from Biozone MNN1 (Chattian), at the top COZ, to Biozone MNP25b (Chattian), at the botton of HDZ; 2) from Biozone MNN1, at the top of HDZ, to Biozone MNP24 (Chattian) recorded at the bottom of undeformed zone (Fig. 7).

HDZ fabric is characterized by well-developed calcite-infused systems of P- and Y-surfaces that are similar to those observed in the core, but distributed with less frequency and intensity (Fig. 11a). However, HDZ lacks the typical asymmetric folding observed pervasively in the core.

As mentioned, Y-planes are sharp, planar shear surfaces marked by thin gouges layers, ranging from N 150° to N 170°, and dipping roughly 40°–50° towards the SW (Fig. 10c). P-type foliation can be described as a variably continuous, anastomosing to locally scaly cleavage, with spacing everywhere greater than 2 mm. The P-planes strike N1 40°–N 180°, with a dipping ranging from 50° towards SW to 80° towards the NE (Fig. 9c). Typically, the P-planes show a change in attitude from high angle to parallelism with the Y-planes (Fig. 11a). As in the fault core, microscopic variably continuous pressure solution seams and elongate rigid grains define the P-foliation. The attitude of P- and Y-planes is interpreted as a top-to-ENE sense for shear of the MRSZ.

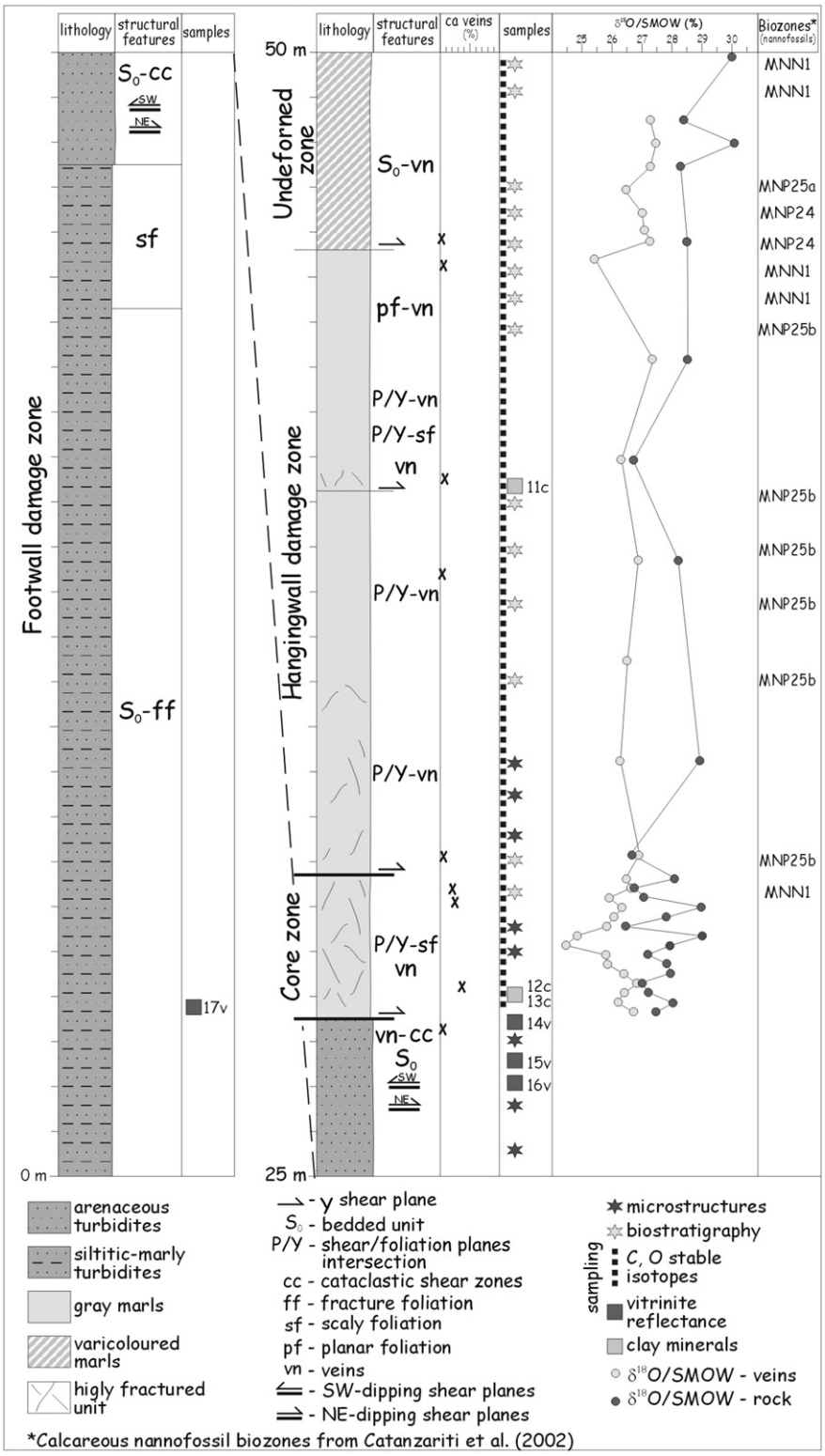

Fig. 7. Structural profile measured across the MRSZ parallel to zone dip direction showing major structural features at meso-scale, vein density, biostratigraphic data and isotopic values.

Although marked by a sharp surface, the transition to the undeformed Monte Rentella Formation is outlined also by a decrease in density of P-Y structures. Moving from the bottom to the top of the HDZ, the spacing of Y-planes changes from 5 to 10 cm to 30–40 cm. An increase in spacing is also observed for the S-planes.

4.2. Mineralization along the MRSZ: mesoscopic and microscopic features

All shear zone components are characterized by abundant vein development, whose density strongly varies from the damage

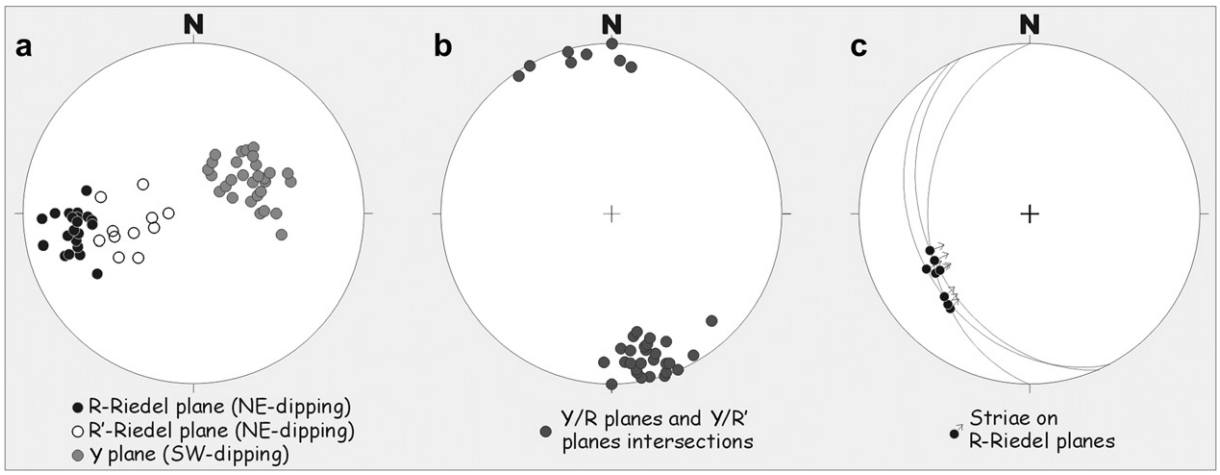

Fig. 8. Lower hemisphere projection of most significant structural elements in the footwall damage-zone sandstones.

zones to the fault core. In addition, veins arrangement and texture also change, depending on the host lithology.

Mineralization in the FDZ sandstones occurs along up to 2 cm thick, Mode I fractures sub-normal to bedding. Vein walls are sharp and planar. The infillings show antitaxial texture, with straight fibres of calcite. The median line is highly discontinuous and, when visible, is marked by either small sandstones chips or simply by the boundary between different calcite crystals (Fig. 11b). Fibres vary greatly in thickness (0.2–0.5 mm) and length (1–4 mm). As it is present only in the damage zone of the footwall, this vein system lacks any particular feature that enables us to relate it directly to the fault zone.

The marls of the core and hangingwall damage zones of the MRSZ are characterized by similar mineralization, but a dramatic decrease in vein density is observed when moving from core to HDZ (Fig. 7), where veins are also less deformed.

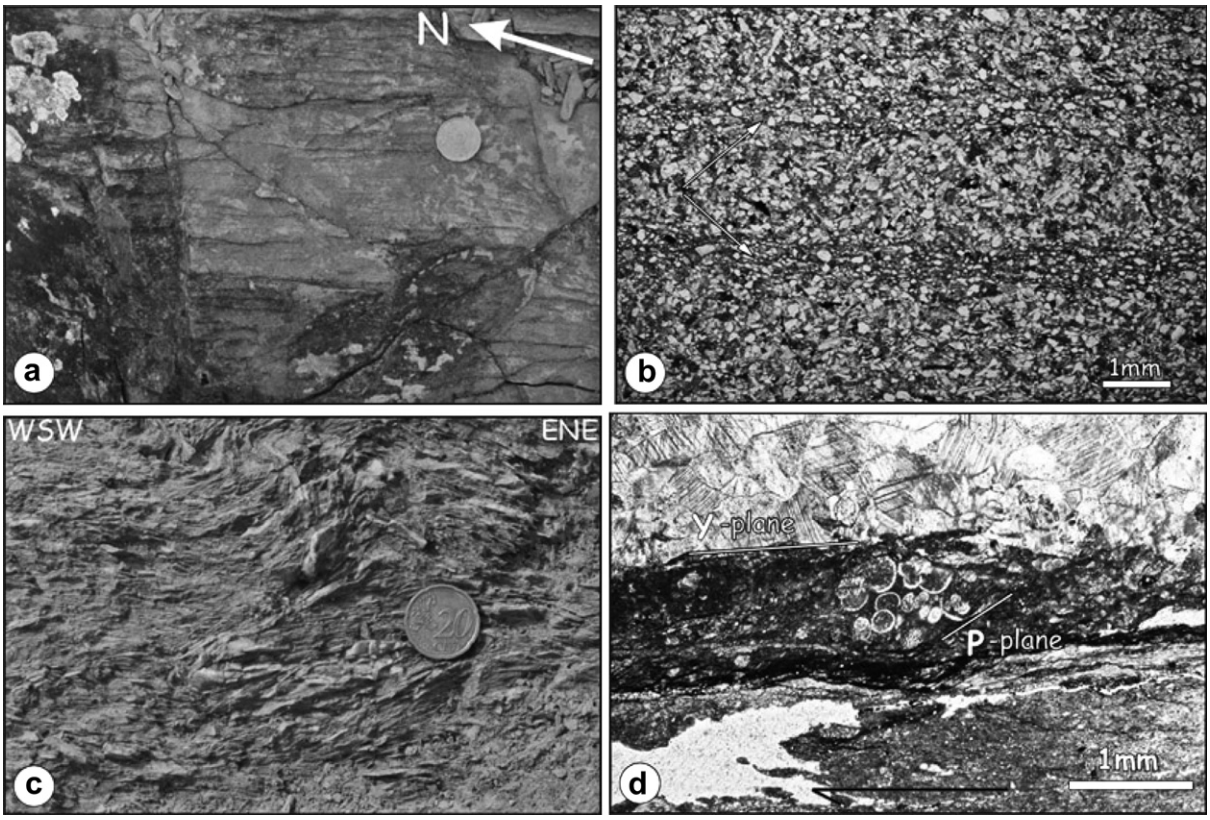

Fig. 9. Main deformation features in the MRSZ. Cataclastic shear zones developed in footwall sandstones at a) field and b) micro-scale (crossed nicols). Cataclastic shear zones (indicated with white arrows) at micro-scale are defined by grain-size reduction associated with pressure solution. Coin diameter is 2 cm c) Deformation of marls in core and hangingwall damage zones are characterized by penetrative scaly foliation, asymmetric folds and veins. Coin diameter is 2 cm. d) Shear sense indicator in marls: P-Y planes sets and asymmetric clasts, all pointing towards a top-to-NE sense of shear.

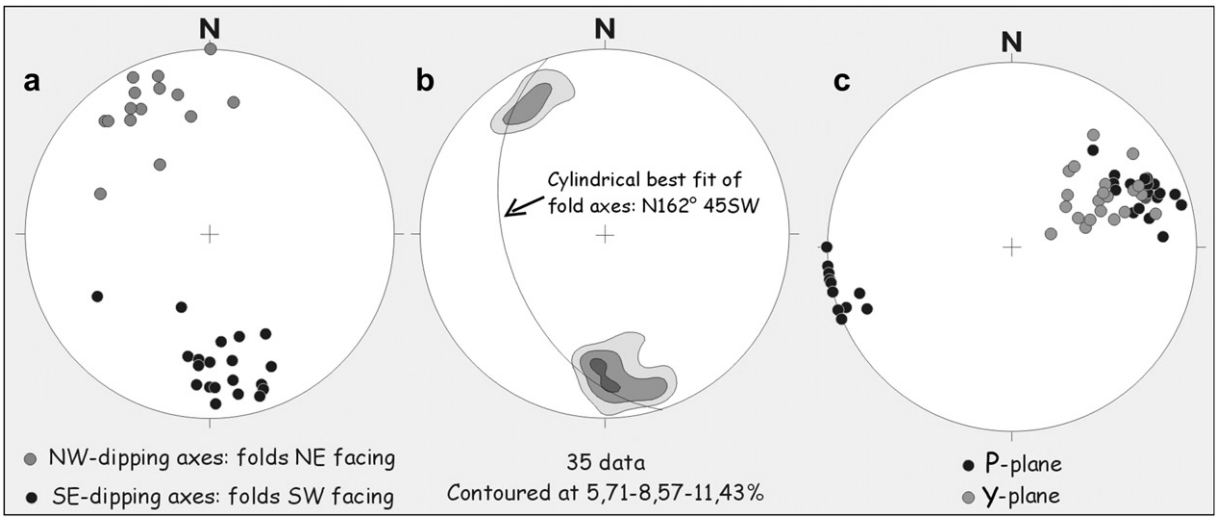

Fig. 10. Lower hemisphere projection of most significant structural elements in the marls of core zone (a and b) and hangingwall damage zone (c).

The calcite veins along the P- and Y-planes in the deformed marls range in thickness from 2 mm to 1 cm in the core and up to 2 cm in the HDZ (Fig. 11a). Y-shear-parallel veins are thicker, planar and continuous, and show sharp boundaries. The foliation-parallel vein system is less developed than the Y-shear parallel ones, especially in the damage zone, and it is less continuous, probably as a result of folding and disruption during shear.

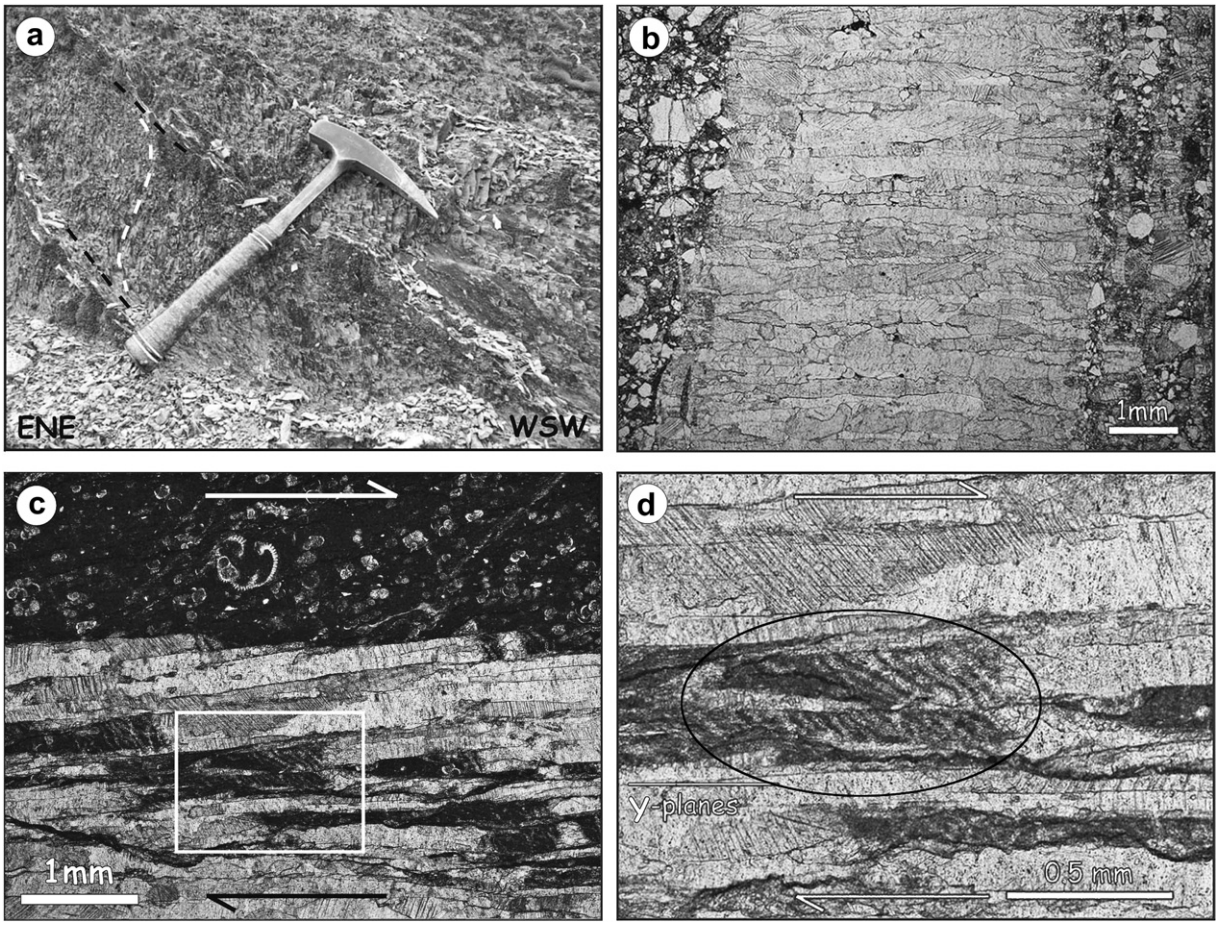

Fig. 11. a) Field-scale image of vein, running along Y-type shear planes (black dashed lines), in damage zone marls. White dashed line mimics foliation deflected by shear surfaces Discontinuous white layers along Y-surfaces are calcite veins. b) Microphotograph of fibrous layer-normal veins in footwall sandstones. c) Striped veins in damage and core zones marls at micro-scale (plane nicols). Veins are arranged along Y-shear planes and are characterized by many crack-and-seal episodes. Staircase geometry visible at vein upper boundary define sense of vein opening and shear. White box is area of Fig. 11d. d) Close up view of vein system (crossed nicols). Different calcite stripes parallel the main vein boundaries and Y-shear surfaces. The centre of microphotograph (circled) shows inclusions of wall-rock marls accommodating further deformation through smaller dilatational jog structures. Top-to-the-NE sense of shear.

Although no particular texture is discernable in the veins at the outcrop scale, vein walls along Y-shears bear a well-developed lineation on calcite crystals trending N 60°–N 110°. Along the Y-surfaces, a progressive change of the trend of the calcite fibres from N 20° to N 90°, locally occurs.

Veins arranged along the Y-shear planes have morphologies consistent with experiencing many crack-and-seal episodes and a texture (Fig. 9d and Fig. 11c-d) comparable to that described for the dilational jogs of Sibson (1987), or for the striped veins of Koehn and Passchier (2000). MRSZ veins show long, thin stripes of calcite crystals, separated by crack-seal bands parallel to the jog where first opening occurred (Fig. 11c). Jogs for different vein episodes show a staircase shape that can be used as a shear sense indicator, and is always consistent with a top-to-the-NE shear sense (Fig. 11c). Grain boundaries of crystals do not track the opening of the veins, the displacement being sub-parallel to the boundaries between different calcite stripes (Fig. 11c–d): these surfaces parallel the main vein boundaries, i.e. the Y-surfaces themselves, and therefore, according to Sibson (1987), Koehn and Passchier (2000), they represent shear surfaces. Typically, along these dark shear surfaces, pressure solution seams also concentrate. Locally, trapped between different crack-seal episodes are inclusions of wall rock marls big enough to be able to accommodate further deformation through smaller dilatational jog structures (Sibson, 1987), which are again consistent with the main top-to-the-NE sense of shear (Fig. 11d).

Y-shear surfaces, and associated veins, are locally arranged in systems that can be fairly well related to specific Riedel shear planes (Fig. 12a). The orientation of R, P and Y surfaces is always compatible with a top-to-the-NE sense of shear.

Following Burkhard's (1993) classification, calcite twins in MRSZ are type II (Fig. 12b), suggesting a qualitative estimate for formation temperature of 150°–300 °C for both vein systems (see also Ferril et al., 2004).

Mineralization along the foliation surfaces (Fig. 12c) is characterized by calcite extension veins with a variable thickness that is up to twice as that of a single "striped episode" along the Y-surfaces. Infilling is fine, clear calcite blocky crystals. As with the foliation planes, the veins are deformed by shear along the Y-planes to give rise to structures resembling S-C structures (Fig. 12c), consistent with top-to-the-NE sense of shear.

Veins in the fault core are frequently deformed and disrupted by shear-related folding. As already described, fold vergence is always consistent with top-to-the-NE sense of shear (Fig. 12d). Locally, repeated folding and shear-related deformation allowed complete disruption of veins, and a brecciated structure (Fig. 12e).

Scanning electron microprobe (SEM) observations of samples of host rock marls from undeformed, damage and core zones suggests local fluid/rock interaction during fault activity and veins precipitation. The SEM images of core zone marl samples, in fact, show extensive precipitation of calcite and quartz, highlighted by a marl microfabric featuring the occurrence of triple junctions and straight boundaries between crystals (Fig. 12f). The amount of recrystallization decreases away from the core zone towards the undeformed marls with granular texture.

4.3. Fluid-rock interaction and temperature conditions of fluids along the MRSZ: the analysis of C and O stable isotopes

Stable isotope analyses allow us to characterize the fluid-rock interaction along thrusts during their evolution, by determining the source of fluids involved and the diffuse or confined nature of fluid flow. For these reasons, we sampled a representative number of deformed marls and carbonate veins developed during MRSZ activity. Vein sampling was performed across the shear zone by selecting veins and adjacent wall rocks in the footwall damage zone, core zone and hangingwall damage zone. Marl samples of Monte Rentella Formation were collected from the undeformed zone up-section from the deformed hangingwall damage zone.

Selected veins were mechanically drilled from polished surfaces. Powdered rocks and veins were reacted with orthophosphoric acid at 25 °C under vacuum for 12 h (McCrea, 1950). The isotopic compositions ($^{13/12}$C and $^{18/16}$O ratios) of the resulting CO_2 have been measured using Thermo-Finnigan Delta XP IRMS at the CNR-IGG of Pisa. Proper standardization for the O- and C-isotope analyses was verified by international carbonate standards, including NBS-19 (calcite), and internal calcite standard. The internal standard (Carrara marble) has uncertainty (expressed as 1σ) less than 0.10‰ for both δ^{18}O and δ^{13}C, and was regularly added to each run of measurement (i.e., 5 samples + 1 internal standard).

The δ^{18}O values for the host rocks of the core and hangingwall damage zone range approximately from 27 to 29‰, (average value for both rock groups = 27.7–27.8‰) (Table 2, Figs. 7 and 13). δ^{13}C of the same samples is quite constant ranging from 0.5 to 1.3 for core samples and from 0.8 to 1.5 for hangingwall host rocks. Additional samples were used to investigate the transition from deformed hangingwall damage zone to undeformed marls (see Fig. 7): δ^{18}O values range from 27 to 30‰ (average value 28.8‰) and δ^{13}C from 0.4 to 1.5‰. Importantly, the MR79(h) rock sample, representing an undeformed marl, shows the highest δ^{18}O value (30‰). Carbonate veins selected and mechanically drilled from the core show δ^{18}O and δ^{13}C values ranging from 24 to 27‰ (average value 26.0‰) and from 0.4 to 1.5‰, respectively. δ^{18}O and δ^{13}C values of hangingwall damage zone carbonate veins (v-HDZ) range from 25 to 27‰ (average value 26.5‰) and from 0.7 to 1.5‰. Carbonate veins from the transitional zone to the undeformed marls show a quite constant δ^{18}O of around 27‰ and δ^{13}C values from 0.7 to 1.3‰.

The rock samples and associated veins from the sandstones of the footwall all show similar δ^{13}C and δ^{18}O values, between 0.1–0.2‰ and 24.7–25.3‰, respectively (Table 2).

5. Discussion

5.1. Strain localization, hydrofracture opening/closure, and their mutual feedback during MRSZ evolution

Deformation in MRSZ mainly concentrated in marls, creating an asymmetric geometry with a wide hangingwall damage zone in the Monte Rentella Formation that progressively grades to the undeformed protolith, whereas, down-section, it sharply passes into a fault core where strain is concentrated and deformation is more penetrative. The MRSZ is a tabular structure where competent rigid blocks of siltite are enclosed in a matrix of marl gouge. This block-in-matrix fabric, together with the occurrence of scaly fabric, systems of P-foliation and Y-shear surfaces, and insoluble oxides seams in marls all indicate that cataclastic flow and pressure solution were the main deformation processes active during thrust evolution (Knipe, 1986, 1989; Lundberg and Moore, 1986; Labaume et al., 1997). The rheological heterogeneity of competent siltite layers alternating with incompetent marls in the Monte Rentella Formation created a heterogeneous distribution of shear strain, and involved both continuous and discontinuous deformation. We believe that viscous flow occurred during deformation in the matrix, so that the strain concentrated at the rigid siltite phacoids boundaries by developing brittle, discrete slip planes, such as the Y-planes, that accommodated most of the displacement along the shear zone (Lister and Williams, 1983; Fagereng and Sibson, 2010). Similar fabrics are typically observed at different scale, in a wide range of crustal, metre-scale fault zones and shear-related mélanges (Sibson, 1977, 1994; 1996; Lundberg and Moore, 1986; Aydin and Schultz, 1990; Labaume et al., 1991; Chester et al., 1993; Antonellini and

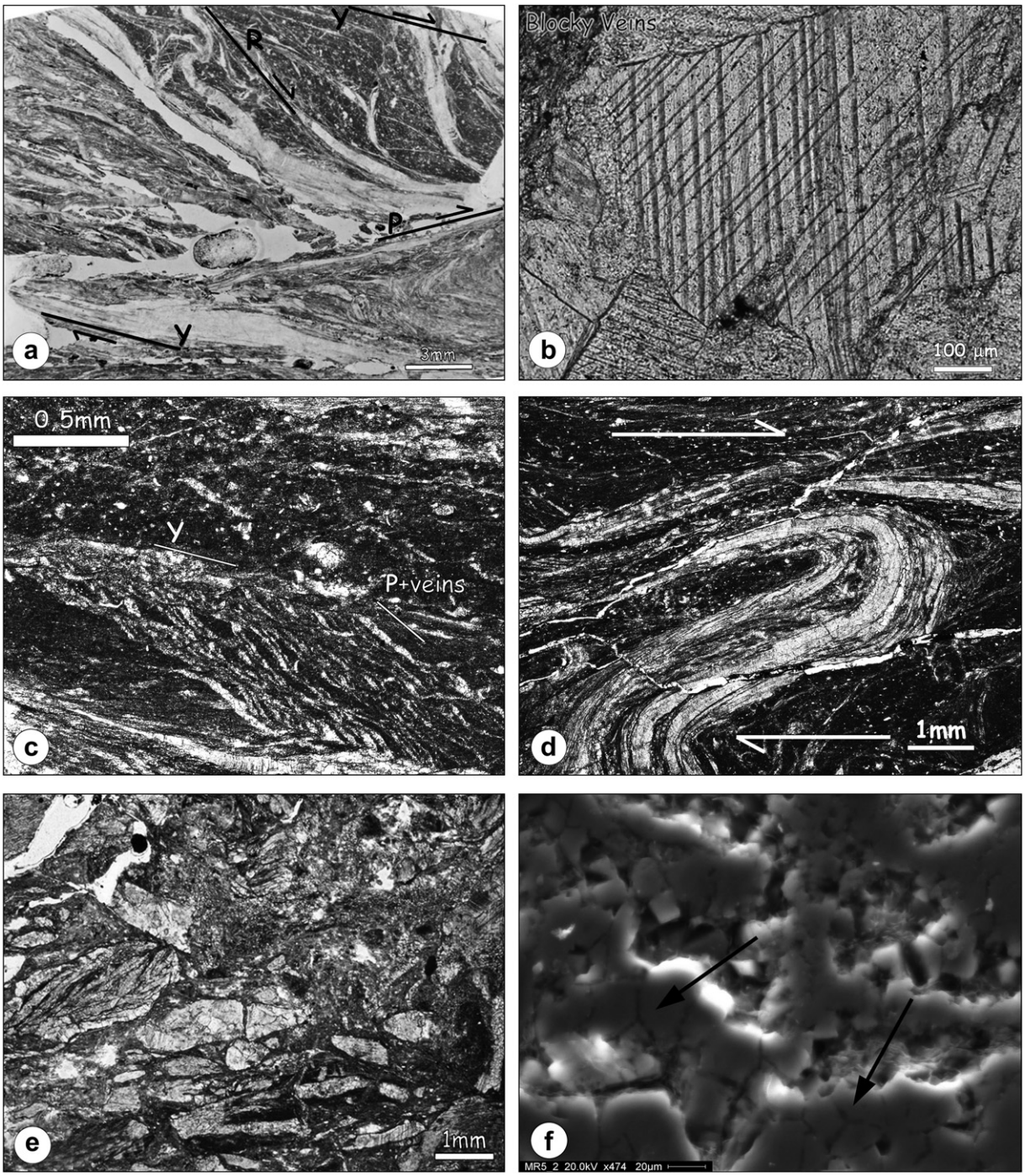

Fig. 12. a) Shear surfaces, and associated veins, are arranged in Riedel shear planes systems in which R, P and Y planes are compatible with a top-to-the-NE sense of shear (photomicrograph, plane nicols). b) Calcite crystals in veins show thin, straight twin lamellae. c) Veins along foliation are extension veins with fine blocky calcite. Along foliation are also pressure solution seams. Foliation surfaces are cut and deformed by Y-shear surfaces to form structures similar to the S-C structures of the ductile regime. d) Deformed striped veins by shear-related isoclinal fold in core marls (photomicrograph, crossed nicols). e) Repeated folding and shear-related deformation allow complete disruption of veins and a brecciated structure (photomicrograph, crossed nicols). f) SEM image (secondary electrons) of host rock marls from the MRSZ core. Recrystallization is suggested by frequent triple junction between crystals (black arrows).

Aydin, 1995; Caine and Forster, 1999; Pini, 1999; Jeanbourquin, 2000; Labaume and Moretti, 2001; Goodwin and Tikoff, 2002; Meneghini and Moore, 2007; Fagereng and Sibson, 2010).

The progressive formation and interconnection of Y- and P-planes with evolving cataclasis and shear yielded a complex fracture mesh (Sibson, 1996). The syntectonic development of the hydrofracture system in both the core and the damage zones of the MRSZ with mineralization preferentially along the Y-shear planes, is interpreted to mean that the mesh worked as a preferential conduit for fluid migration during shear (Fig. 14). The core and the damage zones, therefore, represented distinct mechanical and permeability heterogeneities that focussed fluid flow during thrusting and internal deformation of the entire unit.

As described, the geometry and texture of the MRSZ vein system parallel to the Y-shears resemble the striped veins described by Koehn and Passchier (2000), or the infilling of dilational jogs of

Table 2
Isotopic values of C and O in the host rocks and veins.

Sample no.	Structural position[a]	Sample type	$d^{13}C_{PDB}$ (‰)	$d^{18}O_{PDB}$ (‰)	$d^{18}O_{SMOW}$ (‰)
MR-5 (V)	v-COZ	Vein	0.79	−3.99	26.74
MR8 (V)	v-COZ	Vein	1.39	−4.52	26.20
MR9 (V)	v-COZ	Vein	0.44	−4.32	26.41
MR15 (V)	v-COZ	Vein	0.83	−3.90	26.84
MR17 (V)	v-COZ	Vein	1.41	−4.32	26.40
MR19 (V)	v-COZ	Vein	1.17	−4.86	25.85
MR20 (V)	v-COZ	Vein	1.24	−4.91	25.80
MR23 (V)	v-COZ	Vein	0.54	−6.22	24.45
MR26 (V)	v-COZ	Vein	1.13	−5.85	24.83
MR29 (V)	v-COZ	Vein	1.22	−4.88	25.83
MR37 (V)	v-COZ	Vein	0.77	−4.60	26.12
MR38 (V)	v-COZ	Vein	1.40	−4.37	26.35
MR41a (V)	v-COZ	Vein	0.91	−4.79	25.92
MR41B (V)	v-COZ	Vein	1.19	−4.11	26.62
MR43 (V)	v-COZ	Vein	1.52	−4.24	26.49
MR5 (H)	h-COZ	Host rock	0.53	−3.31	27.45
MR6 (H)	h-COZ	Host rock	0.56	−2.75	28.02
MR13 (H)	h-COZ	Host rock	0.60	−3.54	27.21
MR16 (H)	h-COZ	Host rock	0.74	−3.68	27.07
MR18 (H)	h-COZ	Host rock	1.26	−2.80	27.97
MR21 (H)	h-COZ	Host rock	1.09	−2.95	27.82
MR22 (H)	h-COZ	Host rock	0.67	−3.53	27.22
MR23 (H)	h-COZ	Host rock	0.90	−2.84	27.94
MR27 (H)	h-COZ	Host rock	1.16	−1.76	29.05
MR28 (H)	h-COZ	Host rock	0.99	−4.22	26.51
MR36 (H)	h-COZ	Host rock	1.18	−2.85	27.93
MR40 (H)	h-COZ	Host rock	1.01	−1.81	28.99
MR42a (H)	h-COZ	Host rock	0.55	−3.58	27.17
MR44 (H)	h-COZ	Host rock	1.18	−3.95	26.78
MR46 (H)	h-COZ	Host rock	0.88	−2.68	28.10
MR48 (V)	v- COZ-HDZ	Vein	0.87	−5.04	25.66
MR49 (V)	v - COZ-HDZ	Vein	0.75	−3.71	27.03
MR52 (V)	v - COZ-HDZ	Vein	0.86	−3.92	26.82
MR-51 (V)	v - COZ-HDZ	Vein	1.40	−4.44	26.28
MR53 (V)	h- COZ-HDZ	Host rock	0.85	−4.01	26.72
MR54 (V)	v-HDZ	Vein	1.49	−3.88	26.86
MR56 (V)	v-HDZ	Vein	1.38	−4.47	26.25
MR57 (V)	v-HDZ	Vein	1.19	−4.23	26.50
MR58 (V)	v-HDZ	Vein	1.29	−3.86	26.88
MR60 (V)	v-HDZ	Vein	1.20	−4.44	26.28
MR64 (V)	v-HDZ	Vein	1.23	−3.38	27.37
MR65 (V)	v-HDZ	Vein	0.68	−5.28	25.42
MR53 (H)	h-HDZ	Host rock	0.85	−4.01	26.72
MR55 (H)	h-HDZ	Host rock	1.04	−1.91	28.89
MR59 (H)	h-HDZ	Host rock	1.51	−2.56	28.22
MR62 (H)	h-HDZ	Host rock	0.90	−4.00	26.73
MR64 (H)	h-HDZ	Host rock	1.10	−2.30	28.49
MR67 (V)	v-HDZ-IND	Vein	1.28	−3.51	27.24
MR69 (V)	v-HDZ-IND	Vein	0.96	−3.68	27.06
MR-73 (V)	v-HDZ-IND	Vein	0.95	−3.51	27.24
MR71 (V)	v-HDZ-IND	Vein	0.71	−4.23	26.50
MR75 (V)	v-HDZ-IND	Vein	0.70	−3.32	27.44
MR-77 (V)	v-HDZ-IND	Vein	0.80	−3.54	27.21
MR-70 (V)	v-HDZ-IND	Vein	0.98	−3.71	27.03
MR67 (H)	h-HDZ-UND	Host rock	1.46	−2.3	28.46
MR78 (H)	h-HDZ-UND	Host rock	0.91	−2.4	28.40
MR74 (H)	h-HDZ-UND	Host rock	0.76	−2.5	28.29
MR76 (H)	h-HDZ-UND	Host rock	0.88	−0.8	30.05
MR79 (H)	UND	Host rock	0.9	−1.3	30
MR34 (V)	v-FDZ	Vein	0.06	−5.47	25.23
MR35 (V)	v-FDZ	Vein	0.15	−6.02	24.66
MR34 (H)bis	h-FDZ	Host rock (sandstone)	0.22	−5.35	25.34
MR35 (H)bis	h-FDZ	Host rock (sandstone)	0.19	−5.39	25.31

[a] v: vein; h: host rock; COZ: core zone, HDZ: hangingwall damage zone; FDZ: footwall damage zone; UND: undeformed; COZ-HDZ: core zone - hangingwall damage zone transition; HDZ-UND: hangingwall damage zone - undeformed transition.

Sibson (1987). Both striped veins and dilational jogs typically form when a shear surface is not planar. The occurrence of jogs at high angles to a shear plane allows extension and the creation of voids during each shear event. If fluids infuse a shear zone, then the decay of pressure in the voids may cause precipitation and filling of the voids themselves. The mineralization along the Y-planes in the MRSZ shows multiple striped veins, suggesting multiple opening and closure events along the same fracture. Therefore, as suggested by Ramsay (1980) for crack and seal veins, by Sibson (1981, 1987) for dilational jogs, and as presented in the model of Koehn and Passchier (2000), we believe that the formation of these veins and the regularity of opening events occurred in response to cyclic

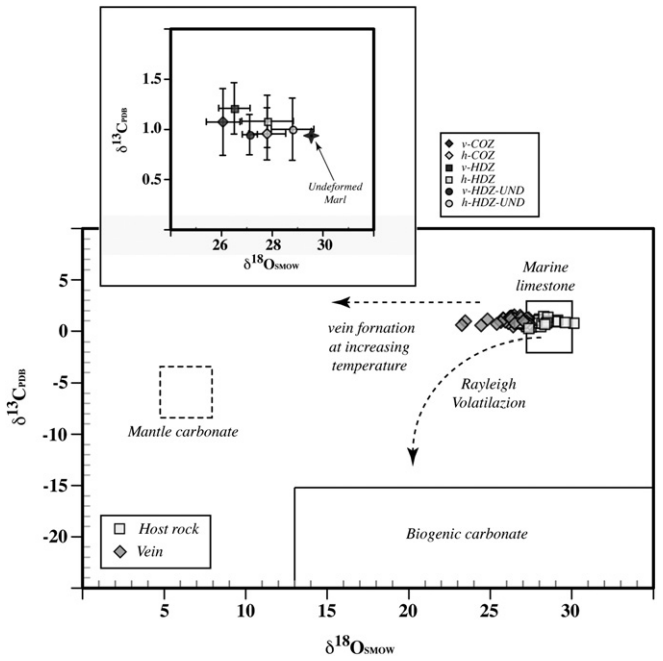

Fig. 13. Carbon and Oxygen isotope data of the Rentella carbonate veins and host rocks (marls): oxygen values are related to (SMOW) and carbon values are related to (PDB). Range of values for biogenic carbonate, marine limestone and mantle carbonate are reported for comparison (data from Hoefs, 2009). The top left inset represents the Carbon and Oxygen isotope average values for the veins and host rocks from the different segments of the thrust system (i.e.: from core zone (COZ), hangingwall damage zone (HDZ) and undeformed zone (UND)) and shows in more detail the data variation.

build-up of fluid overpressure and injection of fluids into the shear zone, roughly synchronous with increments of fault slip. Accordingly, foliation is marked by pressure solution seams, but it is also the locus of extension veins development, confirming the hypothesis of cyclic changes in pore pressure causing alternation of dilation and compression along the same plane (Fig. 12c and Fig. 14).

Although phyllosilicate-rich fault cores of large displacement faults generally show low permeability and represent barriers for fluid flow (Faulkner and Rutter, 2001; Collettini et al., 2006 and references therein), cataclasis and shear in the MRSZ created an irregular mesh of discrete shear surfaces, arranged as Riedel planes, that enabled fluid flow along and across the fault zone (Sibson, 1977, 1996; Sibson, 1987; Byerlee, 1993; Caine and Forster, 1999; Faulkner and Rutter, 2001). Because of the crack and seal vein texture and the mutual relationships with foliation, shear and pressure solution surfaces, we hypothesize that fluid injection was likely cyclic, which would have meant that deformation and slip were likewise cyclic (Sibson, 1987; Vannucchi et al., 2010).

5.2. Nature and temperature of the fluids migrating along the MRSZ

Fluid flow and fluid-rock interactions can leave detectable signatures in rocks, and, depending on the origin of the fluids, on the fluid/rock ratio, the pervasive/localized circulation of fluids and the mineral filling, rocks and associated veins acquire different isotopic signatures (Hoefs, 2009). Consequently, stable isotopes are used to study vein systems so as to identify fluid sources, estimate temperatures of vein formation (for bimineralic veins), and evaluate fluid-rock ratios and processes by which veins form. The $\delta^{13}C$ values constrain the carbon source, whereas the $\delta^{18}O$ values give indirectly information about the aqueous fluids. In this study, we have compared $\delta^{18}O$ and $\delta^{13}C$ of vein fillings with their host to gain additional information about the fluid involved in the shear zone at Monte Rentella.

As shown in Figs. 7 and 13, the stable isotope results highlight a systematic isotopic difference in $\delta^{18}O$, up to 3‰, between host rocks and veins in each structural position across the measured section, while $\delta^{13}C$ is constant for the vein/rock samples. Moreover, a systematic variation in $\delta^{18}O$ values is recorded across the section moving from the undeformed marls to the core of the fault. In summary (Figs. 7 and 13): i) $\delta^{18}O$ values of the carbonate veins are lower than their surrounding host rocks, ii) $\delta^{18}O$ of veins decrease from the undeformed section, to the hangingwall damage zone to the core, and iii) $\delta^{18}O$ in the host rocks samples decrease irregularly

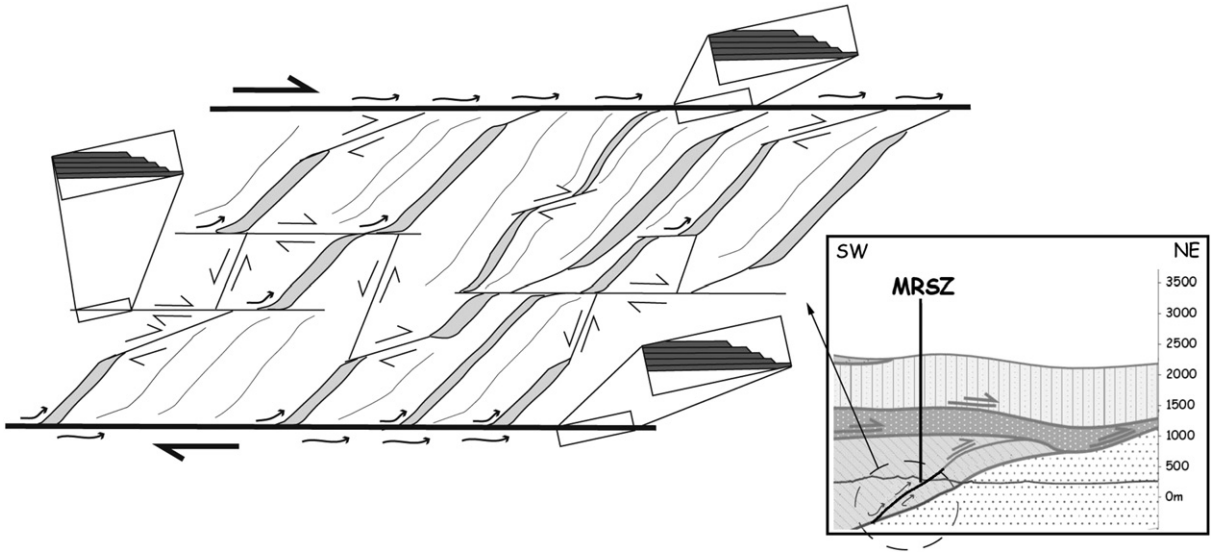

Fig. 14. Schematic representation of the fault-fracture mesh along MRSZ (sketch from Fig. 11c and Fig. 12c). Striped veins (dark grey in the close ups) develop along shear surfaces through a crack-and-seal mechanism at each increment of slip (see Fig. 11c). At the same time, extension veins (light grey) mineralize along foliation planes (thin lines) and are deformed during progressive shear. Parallel to foliation are also surfaces of pressure solution, testifying to alternation of dilation and compaction related to transient changes of fluid pressure. Small arrows indicate fluid migration across discrete surfaces. The inset shows the MRSZ (circled) from Fig. 6 with a representation of the hot fluid migrating along the fault zone from depth (refer to Fig. 6 for patterns in cross section).

from the undeformed section, to the hangingwall damage zone to the core. The last two groups show similar $\delta^{18}O$, 2‰ less than the undeformed end-member.

Concerning the last point, we have shown that the core zone represents a preferential locus for relatively large amount of fluids, as demonstrated by the abundance of carbonate veins. The host rock in the core records the biggest depletion in ^{18}O compared to the same lithology away from the fault zone, suggesting that the circulating fluid interacted strongly with the surrounding rock. In fact, the occurrence of a fossil hydrothermal conduit, channelling large fluxes of fluids, is indicated by a lowering of the $\delta^{18}O$ values of the host rocks surrounding the conduit as compared to the same rock far from the hydrothermal path (Hoefs, 2009). According to a diffusive and progressive fluid/rock interaction, the surrounding damage zone reveals intermediate $\delta^{18}O$ values between the core and the undeformed zone. Moreover, the SEM-scale microfabric of the marls hosting the veins, shows intense recrystallization with triple junctions between crystals in the most deformed, intensely veined fault core, demonstrating a localized interaction of rocks and an external fluid, with high fluid/rock ratio, able to change the isotopic signature and mineralogical characteristic.

$\delta^{18}O_{veins}$ values lower than those of the host rocks suggest that fluids responsible for the veins precipitation were not isotopically buffered by surrounding host rocks and that the system was not closed to external fluids input. Given the occurrence of a constant vein vs. rock O isotope shift, with nearly constant C-isotope compositions, we propose that the external fluid was an oxygen-rich fluid such as H_2O and not a CO_2-rich fluid, and very little, if any, carbon was involved. If we assume a precipitation of $CaCO_3$ and Rentella veins ($\delta^{18}O_{SMOW} = 26–27‰$) in equilibrium with the fluid, the oxygen isotope composition of the fluid, depending on the temperature, would vary from ~9–10‰ (at 100 °C) to ~16–17‰ (at 200 °C; fractionation factors from O'Neil et al., 1969). Such a fluid falls in the range of typical metamorphic isotope values, being very far from other hypothetical fluids, like trapped seawater ($\delta^{18}O_{SMOW} = 0‰$), or pore water (±3‰ seawater value; Hoefs, 2009).

The oxygen isotope composition observed in the MRSZ samples ($\delta^{18}O_{SMOW} = 26–27‰$) could derive from a deep interaction between buried pore fluids (±3‰ seawater value; Hoefs, 2009) and the Rentella marls, producing a partial dissolution of carbonate and generating heavier pore fluids responsible for the calcite veins precipitation at shallow levels. Because marine carbonates generally have $\delta^{18}O$ values higher than any other mineral, virtually any hydrothermal fluids in equilibrium with sedimentary carbonate would show the heaviest $\delta^{18}O$ values. However, to produce carbonate veins with $\delta^{18}O_{SMOW} = 26‰$ from an original source value of 30‰ (Fig. 13), the fluid would have to follow an increasing temperature pathway, such as for example dissolution at lower temperature and re-precipitation at higher temperature; following fractionation factors from O'Neil et al. (1969). This inference is not in agreement with our geological and petrological evidence, and therefore, this hypothesis can be rejected.

The calcite twins in the veins infilling enables a qualitative estimate of temperature, which is 150 °C–300 °C (Burkhard, 1993). Hydrocarbon maturation occurs roughly between 100 °C and 150 °C and transforms solid organic matter to fluid, thus representing another possible source of fluids (Moore and Saffer, 2001). However, the released fluids would be CO_2-rich fluids, which does not fit our data about the carbon isotopes in the veins, which have constant or typically "inorganic" positive values (Fig. 13).

Metamorphic fluids are commonly released at depth, where metamorphic reactions produce mechanical expulsion of large quantities of fluids towards the surface. The geology of the Monte Rentella suggests that the Monte Rentella thrust juxtaposes the Rentella and Montagnaccia Formations (Figs. 2 and 6), both characterized by illite and mixed layers I-S. The smectite to illite transformation appears to be important at about 150 °C (Moore and Vrolijk, 1992; Moore and Saffer, 2001). Since the oxygen isotope composition deduced from the veins lies in the field of metamorphic fluids (Fig. 13), and given this temperature for active transformation, we regard the smectite to illite change as the most probable source of the metamorphic fluids responsible for vein formation along the MRSZ. The temperature of 150 °C needed for this reaction would fit with the qualitative temperature range determined from the calcite twins in the veins, thus representing a minimum estimate for the fluid temperature. Moreover, this interpretation is in accordance with observed and modelled behaviour in ancient shallow-level thrusts and accretionary units involving similar lithologies (Vrolijk et al., 1990; Moore and Vrolijk, 1992; Moore and Saffer, 2001; Vannucchi et al., 2010).

In summary, all these observation point to an intense involvement of externally-derived fluids, with temperature of 150–200 °C and focused mainly in the core zone, that produced a precipitation of carbonate veins, a depletion in ^{18}O of the host rocks and a pervasive precipitation of calcite + quartz in core host-rock samples. Diagenetic reactions such as the smectite to illite transformation are proposed as the possible source of fluids at depths.

The isotopic values of vein samples and adjacent host rocks from the sandstone footwall damage zone all fall into the same field and are not congruent with the data from the marls of the core and hangingwall damage zones. Similar isotopic values in host rock and veins suggest a local mechanism of dissolution-reprecipitation, with the fluids being isotopically buffered by the sandstones. Therefore, we consider the fluid circulation responsible for vein precipitation in the sandstones as unrelated to the external fluid input of fluids envisaged for the marls.

6. Conclusions

The new set of structural, isotopical and thermal maturity data presented in this study provides a snapshot into fluid regime and evolution during fault activity in a collisional setting. While fluid release and circulation are universally recognized as dominating the shallow levels of subduction, their involvement in faulting during the collisional phases is not very well documented in literature.

Similarly to the behaviour along subduction margins, our thrust fault example evolved through cycles of compaction and dilation linked to transient build-up of fluid overpressure and injection (Sibson, 1987; Koehn and Passchier, 2000; Vannucchi et al., 2010). Fluids mineralized with a crack-and-seal mechanism in shear veins with the opening direction at a low angle with the main shear surfaces (and Y-planes). Extension veins along foliation surfaces connected shear surfaces to form a fault-fracture mesh that worked as a preferential fluid conduit during slip (Fig. 14).

While the thrust was active at very shallow depths, with maximum paleotemperatures in the early diagenetic zone and in the immature to early-mature stages of hydrocarbon generation (ca. less than 3 km), blocky and striped veins both formed from fluids with warmer temperature conditions of 150°–200 °C. We envision the source area for hot fluids to be located at deeper structural levels in the collisional prism, where diagenetic and low-grade metamorphic reactions could produce fluids by dehydration of clay minerals. The hot fluids pumped from the deeper portions of the collisional prisms strongly interacted with the host rocks, modifying not only their isotopic character, but also their local texture at micro-scale.

Acknowledgements

This research was supported by M.I.U.R (Project PRIN). We are thankful to the Editor William Dunne, to Kotharo Ujiie and to the anonymous reviewer, for their thorough comments that helped to improve the paper. Francesca Meneghini thanks J.C. Moore for comments and suggestions. Chiara Boschi thanks L. Dallai for fruitful discussions and E. Calvi for assistance with carbonate lab.

References

Aldega, L., Botti, F., Corrado, S., 2007. Clay mineral assemblages and vitrinite reflectance in the Laga Basin (Central Apennines, Italy): what do they record? Clays and Clay Minerals 55, 504–518 October.

Aldega, L., Corrado, S., Di Paolo, L., Somma, R., Maniscalco, R., Balestrieri, M.L., 2011. Shallow burial and exhumation of the Peloritani Mts. (NE Sicily, Italy): insight from paleo-thermal and structural indicators. Geological Society of America Bulletin 123, 132–149.

Antonellini, M.A., Aydin, A., 1995. Effect of faulting on fluid flow in porous sandstones: geometry and spatial distribution. American Association of Petroleum Geologists Bulletin 79, 642–671.

Aydin, A., Schultz, R.A., 1990. Effect of mechanical interaction on the development of strike–slip faults with échelon patterns. Journal of Structural Geology 12, 123–129.

Bangs, N.L.B., Shipley, T.H., Moore, J.C., Moore, G.F., 1999. Fluid accumulation and channeling along the northern Barbados Ridge décollement thrust. Journal of Geophysical Research 104, 20399–20414.

Bangs, N.L.B., Shipley, T.H., Gulick, S.P.S., Moore, G.F., Kuromoto, S., Nakamura, Y., 2004. Evolution of the Nankai Trough décollement from the trench into the seismogenic zone: inferences from three-dimensional seismic reflection imaging. Geology 32, 273–276.

Barchi, M.R., De Fayter, A., Magnani, M.B., Minelli, G., Pialli, G., Sotera, B.M., 1998. The structural style of the Umbria-Marche fold and thrust belt. Memorie della Società Geologica Italiana 52, 557–578.

Barchi, M.R.,L., Landuzzi, A., Minelli, G., Pialli, G., 2001. Outer Northern Apennines. In: Vai, G.B., Martini, I.P. (Eds.), Anatomy of an Orogen: The Apennines and Adjacent Mediterranean Basin. Kluwer Academic Publishers, pp. 215–254.

Barker, C.E., Pawlewicz, M.J., 1994. Calculation of vitrinite reflectance from thermal histories and peak temperatures. A comparison of methods. In: Mukhopadhyay, P.K., Dow, W.G. (Eds.), Vitrinite Reflectance as a Maturity Parameter: Applications and Limitations. ACS Symposium Series, vol. 570, pp. 216–229.

Barsella, M., Boscherini, A., Botti, F., Marroni, M., Meneghini, F., Motti, A., Palandri, S., Pandolfi, L., 2009. Oligocene-Miocene foredeep deposits in the Trasimeno Lake area (Central Italy): insights in the evolution of the Northern Apennines. Italian Journal of Geosciences 128, 341–352. doi:10.3301/IJG.2009.128.2.341.

Borrego, A.G., Araujo, C.V., Balke, A., Cardott, B., Cook, A.C., David, P., Flores, D., Hámor-Vidó, M., Hiltmann, W., Kalkreuth, W., Koch, J., Kommeren, C.J., Kusc, J., Ligouis, B., Marques, M., Mendonça Filho, J.G., Misz, M., Oliveira, L., Pickel, W., Reimer, K., Ranasinghe, P., Suárez-Ruiz, I., Vieth, A., 2006. Influence of particle and surface quality on the vitrinite reflectance of dispersed organic matter: comparative exercise using data from the qualifying system for reflectance analysis working group of ICCP. International Journal of Coal Geology 68, 151–170.

Brown, K.M., Saffer, D.M., Bekins, B.A., 2001. Smectite diagenesis, pore-water freshening, and fluid flow at the toe of the Nankai wedge. Earth and Planetary Science Letters 194, 97–109. doi:10.1016/S0012-821X(01)00546-5.

Burkhard, M., 1993. Calcite twins, their geometry, appearance, and significance as stress-strain markers and indicators of tectonic regime: a review. Journal of Structural Geology 15, 351–368.

Byerlee, J.D., 1993. Model for episodic flow of high-pressure water in fault zones before earthquakes. Geology 21, 303–306.

Caine, J.S., Forster, C.B., 1999. Fault zone architecture and fluid flow: insights from field data and numerical modelling. In: Haneberg, W., et al. (Eds.), Faults and Sub-surface Fluid Flow in the Shallow Crust: American Geophysical Union Geophysical Monograph, vol. 113, pp. 101–127.

Chester, F.M., Evans, J.P., Biegel, R.L., 1993. Internal structure and weakening mechanisms of the San Andreas fault. Journal of Geophysical Research 95, 771–786.

Collettini, C., De Paola, N., Goulty, N.R., 2006. Switches in the minimum compressive stress direction induced by overpressure beneath a low-permeability fault zone. Terra Nova 18, 163–231.

Conti, A., Turpin, L., Polino, R., Mattei, M., Zuppi, G.M., 2001. The relationship between evolution of fluid chemistry and the style of brittle deformation: examples from the Northern Apennines (Italy). Tectonophysics 330, 103–117.

Corrado, S., Aldega, L., Di Leo, P., Giampaolo, C., Invernizzi, C., Mazzoli, S., Zattin, M., 2005. Thermal maturity of the axial zone of the southern Apennines fold-and-thrust belt (Italy) from multiple organic and inorganic indicators. Terra Nova 17, 56–65.

Costa, E., Pialli, G., Plesi, G., 1998. Foreland basins of the Northern Apennines: relationships with passive subduction of the Adriatic lithosphere. Memorie Della Società Geologica Italiana 52, 595–606.

Cox, S.F., Wall, V.J., Etheridge, M.,A., Potter, T.F., 1991. Deformational and metamorphic processes in the formation of mesothermal vein-hosted gold deposits: examples from the Lachlan Fold Belt in central Victoria, Australia. Ore Geology Review 6, 391–423.

Cox, S.F., Braun, J., Knackstedt, M.A., 2001. Principles of structural control on permeability and fluid flow in hydrothermal systems. Reviews in Economic Geology 14, 1–24.

Dalla Torre, M., Ferreiro Mählmann, R., Ernst, W.G., 1997. Experimental study on the pressure dependence of vitrinite maturation. Geochimica et Cosmochimica Acta 61, 2921–2928.

Davis, D., Suppe, J., Dahlen, F.A., 1983. Mechanics of fold-and-thrust belts and accretionary wedges. Journal of Geophysical Research 88 (B2), 1153–1172.

Dow, W.G., 1977. Kerogen studies and geological interpretation. Journal of Geochemical Explorer 7, 79–99.

Evans, J.P., Chester, F.M., 1995. Fluid-rock interaction in faults of the San Andreas system: inferences from San Gabriel fault rock geochemistry and microstructures. Journal of Geophysical Research 100, 13,007–13,020. doi:10.1029/94JB02625.

Fagereng, A., Sibson, R.H., 2010. Mélange rheology and seismic style. Geology 38, 751–754. doi:10.1130/G30868.1.

Faulkner, D.R., Rutter, E.H., 2001. Can maintenance of overpressured fluids in large strike-slip fault zones explain their apparent weakness? Geology 29, 203–506.

Ferrill, D.A., Morris, A.P., Evans, M.A., Burkhard, M., Groshong, R.H., Onasch, C.M., 2004. Calcite twin morphology: a low temperature deformation geothermomenter. Journal of Structural Geology 26, 1521–1529.

Fisher, D.M., Brantley, S.L., 1992. Models of quartz overgrowth and vein formation: deformation and episodic fluid flow in an ancient subduction zone. Journal of Geophysical Research 97, 20043–20061.

Fisher, D.M., 1996. Cyclic fluid flow in the forearc: evidence from fabrics and veins. In: Bebout, G., Scholl, D., Kirby, S. (Eds.), Subduction-Top to Bottom, vol. 96. American Geophysical Union Monograph, Washington, DC, pp. 75–90.

Fournier, R.O., 1991. The transition from hydrostatic to greater than hydrostatic fluid pressures in presently active hydrothermal systems in crystalline rock. Geophysical Research Letters 18, 955–958.

Fyfe, V.S., Price, N.J., Thompson, A.B., 1978. Fluids in the Earth's Crust. Elsevier, Amsterdam, p. 383.

Fyfe, W.S., Kerrich, R., 1985. Fluids and thrusting. Chemical Geology 49, 353–362.

Goldstein, A., Selleck, B., Valley, J.W., 2005. Pressure, temperature, and composition history of syntectonic fluids in a low-grade metamorphic terrane. Geology 33, 421–424. doi:10.1130/G21143.1.

Goodwin, L.B., Tikoff, B., 2002. Competency contrast, kinematics and the development of foliations and lineations in the crust. Journal of Structural Geology 24, 1065–1085.

Hilgers, C., Kirschner, D.L., Breton, J.P., Urai, J.L., 2006. Fracture sealing and fluid overpressures in limestones of the Jabal Akhdar dome, Oman mountains. Geofluids 6, 168–184.

Hill, D.P., 1977. A model for earthquake swarms. Journal of Geophysical Research 82, 347–352.

Hillis, R.R., 2001. Coupled changes in pore pressure and stress in oil fields and sedimentary basins. Petroleum Geoscience 7, 419–425.

Hickman, S., Sibson, R.H., Bruhn, R., 1995. Mechanical involvement of fluids in faulting. Journal of Geophysical Research 100, 12,831–12,840.

Hoefs, J., 2009. Stable Isotope Geochemistry, sixth ed. Springer-Verlag, Berlin, p. 285.

Hubbert, M.K., Rubey, W.W., 1959. Role of fluid pressure in mechanics of overthrust faulting. Geological Society of America Billetin 70, 115–166.

Hunt, J.M., 1990. Generation and migration of petroleum from abnormally pressured fluid compartments. Bulletin of the American Association of Petroleum Geologists 74, 1–12.

Jeanbourquin, P., 2000. Chronology of deformation of a Franciscan mélange near San Francisco (California, U.S.A. Eclogae Geologicae Helvetiae 93, 363–378.

Kastner, M., Elderfield, H., Martin, J.B., 1991. Fluids in Convergent Margins – What Do We Know about Their Composition, Origin, Role in Diagenesis and Importance for Oceanic Chemical Fluxes, vol. A335. Philosophical Transaction of the Royal Society of London, pp. 243–259.

Kirschner, D.L., Sharp, Z.D., Masson, H., 1995. Oxygen isotope thermometry of quartz-calcite veins: unraveling the thermal-tectonic history of the subgreenschist facies Morcles nappe (Swiss Alps). Geological Society of America Bulletin 107, 1145–1156.

Knipe, R.J., 1986. Deformation mechanism path diagrams for sediments undergoing lithification. In: Moore, J.C. (Ed.), Structural Fabric in Deep Sea Drilling Project Cores from Forearcs, vol. 166. Memoir of the Geological Society of America, pp. 151–160.

Knipe, R.J., 1989. Deformation mechanisms: recognition from natural tectonites. Journal of Structural Geology 11, 127–146.

Koehn, D., Passchier, C.W., 2000. Shear sense indicators in striped bedding veins. Journal of Structural Geology 22, 1141–1151.

Labaume, P., Berty, C., Laurent, Ph., 1991. Syn-diagenetic evolution of shear structures in superficial nappes: an example from the Nothern Appennines (NW Italy). Journal of Structural Geology 13, 385–398.

Labaume, P., Moretti, I., 2001. Diagenesis-dependence of cataclastic thrust fault zone sealing in sandstones. Example from the Bolivian Sub-Andean Zone. Journal of Structural Geology 23, 1659–1675.

Labaume, P., Maltman, A., Bolton, A., Tessier, D., Ogawa, Y., Takizawa, S., 1997. Scaly fabrics in sheared clays from the décollement zone of the Barbados accretionary

prism. In: Shipley, T.H., Ogawa, Y., Blum, P., Bahr, J.M. (Eds.), Proceedings of the Ocean Drilling Program. Scientific Results, vol. 156, pp. 59–77.
Lavecchia, G., Minelli, G., Pialli, G., 1987. Contractional and extensional tectonics along the transect Lake Trasimeno-Pesaro (central Italy). In: Boriani, A., Bonafede, M., Piccardo, G.B., Vai, G.B. (Eds.), The Lithosphere in Italy. Advanced in Earth Sciences Research, vol. 80. Accademia Nazionale dei Lincei, pp. 177–194.
Law, B.E., Ulmishek, G.F., Slavin, V.I., 1998. Abnormal Pressure in Hydrocarbon Environments, vol. 70. AAPG Memoir, Tulsa, p. 264.
Leader, L.D., Robinson, J.A., Wilson, C.J.L., 2010. Role of faults and folding in controlling gold mineralisation at Fosterville, Victoria. Australian Journal of Earth Sciences 57 (2), 259–277.
Lewis, J.C., Byrne, T.B., Pasteris, J.D., London, D., Morgan, G.B., 2000. Early tertiary fluid flow and pressure-temperature conditions in the Shimanto accretionary complex of southwest Japan: constraints from fluid inclusions. Journal of Metamorphic Geology 18, 219–333.
Lister, G.S., Williams, P.F., 1983. The partitioning of deformation in flowing rock masses. Tectonophysics 92, 1–33.
Lundberg, N., Moore, J.C., 1986. Macroscopic structural features in Deep Sea Drilling Project cores from forearc regions. In: Moore, J.C. (Ed.), Structural Fabric in Deep Sea Drilling Project Cores from Forearcs, vol. 166. Geological Society of America Memoir, pp. 13–44.
Marroni, M., Meneghini, F., Pandolfi, L., 2010. Anatomy of the Ligure-Piemontese subduction system: evidence from Late Cretaceous–middle Eocene convergent margin deposits in the Northern Apennines, Italy. International Geology Review 1, 1–33.
McCrea, J.M., 1950. On the isotopic chemistry of carbonates and a paleotemperature scale. Journal of Chemical Physics 18, 849–857.
Meneghini, F., Moore, J.C., 2007. Deformation and hydrofracture in a subduction thrust at seismogenic depths: the Rodeo Cove thrust zone, Marin Headlands, California. Geological Society of America Bulletin 119 (1), 174–183.
Meneghini, F., Marroni, M., Pandolfi, L., 2007. Fluid flow during accretion in sediment-dominated margins: evidence of a high-permeability fossil fault zone from the Internal Ligurian accretionary units of the Northern Apennine, Italy. Journal of Structural Geology 29, 515–529.
Merriman, R.J., Frey, M., 1999. Patterns of very low-grade metamorphism in metapelitic rocks. In: Frey, M., Robinson, D. (Eds.), Low-grade Metamorphism. Blackwell, Oxford, pp. 61–107.
Moore, D.M., Reynolds Jr., R.C., 1997. X-ray Diffraction and the Identification and Analysis of Clay Minerals. Oxford University Press, New York, p. 378.
Moore, J.C., Vrolijk, P., 1992. Fluids in accretionary prisms. Reviews of Geophysics 30, 113–135.
Moore, J.C., Saffer, D., 2001. Updip limit of the seismogenic zone beneath the accretionary prism of southwest Japan: an effect of diagenetic to low-grade metamorphic processes and increasing effective stress. Geology 29, 183–186.
Moore, J., Orange, D., Kulm, L., 1990. Interrelationship of fluid venting and structural evolution: alvin observations from the frontal accretionary prism. Journal of Geophysical Research 95, 8795–8808.
Newhouse, W.H., 1942. Ore Deposits as Related to Structural Features. Princeton University Press, Princeton, New Jersey.
O'Neil, J.R., Clayton, R.N., Mayeda, T.K., 1969. Oxygen isotopes fractionation in divalent carbonates. Journal of Chemical Physics 51, 5547–5558.
Pauselli, C., Barchi, M., Federico, C., Magnani, M.B., Minelli, G., 2006. The crustal structure of the Northern Apennines (Central Italy): an insight by the Crop03 seismic line. American Journal of Science 306, 428–450.
Pini, G.A. (Ed.), 1999. Tectosomes and Olistrostromes in the Argille Scagliose of the Northern Apennines, Italy. Geological Society of America, Boulder, Colorado, p. 70.
Ramsay, J.G., 1980. The crack-seal mechanism of rock deformation. Nature 284, 135–139.
Rowe, C.D., Meneghini, F., Moore, J.C., 2009. Fluid-rich damage zone of an ancient out-of-sequence thrust, Kodiak Islands, Alaska. Tectonics 28, TC1006. doi:10.1029/2007TC002126.
Saffer, D.M., Bekins, B.A., 2002. Hydrologic controls on the morphology and mechanics of accretionary wedges. Geology 30, 271–274.
Shipley, T.H., Ogawa, Y., Blum, P., The Shipboard Scientific Party, 1995. Northern Barbados Ridge, Leg 156 of the cruises of the Drilling Vessel JOIDES Resolution, Sites 947e949. Proceedings of the ODP, Initial Reports, 156, College Station, Texas (Ocean Drilling Program).
Sibson, R.H., 1977. Fault rocks and fault mechanisms. Journal of the Geological Society of London 133, 191–213.
Sibson, R.H., 1981. Fluid flow accompanying faulting: field evidence and models. In: Simpson, D.W., Williams, P.G. (Eds.), Earthquake Prediction: An International Review. American Geophysical Union, Maurice Ewing Series, vol. 4, pp. 593–603.
Sibson, R.H., 1987. Earthquake rupturing as a mineralizing agent in hydrothermal systems. Geology 15, 701–704.
Sibson, R.H., 1990. Conditions for fault-valve behaviour. In: Knipe, R.J., Rutter, E.H. (Eds.), Deformation Mechanisms, Rheology and Tectonics. Geological Society of London, Special Publication, vol. 54, pp. 15–28.
Sibson, R., 1994. An assessment of field evidence for "Byerlee" friction. Pure and Applied Geophysics 142, 645–662.
Sibson, R.H., 1996. Structural permeability of fluid-driven fault-fracture meshes. Journal of Structural Geology 18, 1031–1042.
Sibson, R.H., 2001. Seismogenic framework for hydrothermal transport and ore deposition. Society of Economical Geology Review 14, 25–50.
Stach, E., Mackowsky, M.Th., Teichmüller, M., Taylor, G.H., Chandra, D., Teichmüller, R., 1982. Stach's Textbook of Coal Petrology. Gerbrüder Borntraeger, Berlin-Stuttgart, p. 535.
Vannucchi, P., Remitti, F., Bettelli, G., Boschi, C., Dallai, L., 2010. Fluid history related to the early Eocene-middle Miocene convergent system of the Northern Apennines (Italy): constraints from structural and isotopic studies. Journal of Geophysical Research 115, B05405. doi:10.1029/2009JB006590.
Vrolijk, P., Chambers, S.R., Gieskes, J.M., O'Neil, J.R., 1990. Stable isotope ratios of interstitial fluids from the Northern Barbados accretionary prism, ODP Leg 110. In: Moore, J.C., Mascle, A. (Eds.), Proceedings of the Ocean Drilling Program, Scientific Results, vol. 110. Ocean Drilling Program, College Station, Tex, pp. 189–205.